

**Predictive method for fires in CLT and glulam structures –
A priori modelling versus real scale compartment fire tests
& an improved method**

Daniel Brandon, Alastair Temple, Johan Sjöström

RISE Report 2021:63

**Predictive method for fires in CLT and glulam structures –
A priori modelling versus real scale compartment fire tests**

Daniel Brandon, Alastair Temple, Johan Sjöström

Abstract

Predictive method for fires in CLT and glulam structures – A priori modelling versus real scale compartment fire tests

Predictive modelling of the fire duration, fire temperatures, heat release rates and the structural capacity during building fires can be used to show compliance with performance-based building code requirements. The predictive models presented in this report focusses on the post flashover fire including the decay phase and extinction of flaming combustion for mass timber structures. *A priori* predictions of five recent compartment fire tests have been set against experimental results and compared. After the tests, the model has been updated, mostly for increased ease of use and increased accuracy for the decay phase.

The model consists of a single-zone model which uses an energy equilibrium approach to obtain gas temperatures and surface temperatures of compartment boundaries. The energy contribution of charring mass timber is included using through-depth temperature calculations of the structure and experimental relationships to determine the combustion rate. The through-depth temperatures of mass timber members also serve to provide information for structural calculations using temperature dependent reduced material properties. However, the structural calculations are out of the scope of the current report.

The radiation conditions (and total thermal exposure to walls ceilings and floors) predicted by the updated model were accurately described the of recent full-scale experiments within the variations between and within the tests. The comparisons with experiments showed that the total heat is, however, underestimated in some cases and surface temperatures were underestimated in the decay phase. Local effects caused by a radiative feedback loop between surfaces that show significant char oxidation, which occurred in a part of the test, is not included in the model.

Key words: CLT, glulam, mass timber, fire, modelling, predictions, performance-based design, structural calculations, natural fires, physically based fires.

RISE Research Institutes of Sweden AB

RISE Report 2021:63
ISBN:978-97-89385-53-5
Borås, 2021

Content

Abstract	1
Content	2
Preface	3
1 Introduction	4
2 The model	4
2.1 Overview	4
2.2 Model Changes.....	7
3 Experiments for comparisons	10
4 A <i>priori</i> modelling predictions according to Brandon and Andersson	11
5 Updated model of this study	14
5.1 Test 4 - large opening predictions	21
5.2 Areas for further improvements	23
6 Conclusions	24
References	26
Annex A: Updated Single Zone Model	28
A.1: Step 1 – Calculate fire temperature time history using an equilibrium approach	28
A.2: Step 2 – Calculate temperatures of all timber members	31
A.3: Step 3– Calculate the charring rate and the corresponding mass timber contribution	34
A.4: Step 4– Add the mass timber contribution.....	35
A.5 Iterative procedure	37
Annex B: Defining the movable fuel load fire	38
B.1 Review of Experimental Data	38
B.2 Maximum heat release rate and external flaming.....	39
B.3 Fire growth rate	39
B.4 Combustion efficiency	39
B.5 The decay phase and the start of decay	40
B.6 Empirical constants.....	40
Annex C: a <i>priori</i> modeling prediction results	43
C.1 Test 1 <i>a priori</i> model predictions	44
C.2 Test 2 <i>a priori</i> model predictions.....	45
C.3 Test 3 <i>a priori</i> model predictions.....	46
C.4 Test 5 <i>a priori</i> model predictions.....	47

Preface

This report provides predictive modeling results of a research project of fire safe implementation of visible wood in tall timber buildings. The main funder of the project is the **US Forest Service (USFS)**, **US Department of Agriculture** (*USFS Grant Number 2019-DG-11083150-022*), the project owner is the **American Wood Council (AWC)**, and **Research Institutes of Sweden (RISE)** is the contractor for this research project. RISE has also provided additional funding for further development of the predictive model of this report

Additional funders of the project are: **Katerra** providing ANSI/APA PRG 320 (2018) compliant CLT, **KLH** providing ANSI/APA PRG 320 (2018) compliant CLT; **Henkel** providing the required ANSI/APA PRG 320 (2018) compliant timber adhesive and additional funding, **Boise Cascade** providing ANSI A 190.1-2017 compliant glued laminated timber; **USG**, providing Type X gypsum boards; **Rothoblaas**, providing mass timber screws, sealants, tapes, resilient profiles and equipment for lifting anchors mass timber members; the **Softwood Export Council** providing shipment costs of US products to the test site in Sweden; **Brandforsk** providing **additional** funding for the inclusion of façade extension measurements. The façade measurements are out of the scope of this report. Technical in-kind contributions were provided by **NIST** for recording of videos in severe fire conditions.

A Steering Group was assembled for this project, comprising of:

Kevin Naranjo (USDA)

Kuma Sumathipala, Jason Smart, Kenneth Bland (AWC)

Sean DeCrane (Building & Life Safety Technologies, UL)

Gordian Stapf, Christian Lehringer, Daniel Current, Chris Whelan (Henkel)

Hans-Erik Blomgren (Katerra)

Sebastian Popp, Johannes Habenbacher (KLH)

Kyle Flondor, Ajith Rao, Young-Geun You (USG)

Susan Jones (Atelier Jones)

Rodney McPhee (Canadian Wood Council)

Dan Cheney (Boise Cascade)

Hannes Blaas, Andres Reyes, Paola Brugnara (Rothoblaas)

All steering group members provided in-kind technical contributions in this project.

1 Introduction

Mass timber is an increasingly popular structural material for large and tall buildings and has been cited for its architectural desirability and low climate impact in comparison with more conventional construction materials.

As mass timber is combustible, implementation of mass timber involves a number of fire safety challenges. Due to a combination of the limited reach of the fire brigade and increased potential consequences, in some countries it is required to ensure fires in taller buildings decay or extinguish using a performance-based approach. In other countries a prescriptive building code is implemented, which often includes protection requirements for mass timber and limits of exposed surfaces. Some countries allow both prescriptive and performance-based fire safety design approaches.

For a performance-based approach, a small number of models have been proposed for engineering use to predict the exposures of flashover fires with exposed surfaces of mass timbers. Parametric fire models were proposed by Barber (2016) and Brandon (2018). A single zone model was proposed by Brandon (2016), which was further developed by Hopkins et al. (2017) and Brandon and Andersson (2018). Wade et al (2019) incorporated the addition of combusting exposed mass timber surfaces in a 2-zone model, B-RISK, with options to perform probabilistic analyses. Schmid et al (2021) developed a plugin for existing zone model software to include the energy contribution of CLT and other mass timber elements.

In the work presented in this report, firstly, a slight adaptation of the model by Brandon and Andersson (2018), is evaluated by comparing previous *a priori* predictions of compartment tests with the corresponding experimental results. Secondly, an updated model using mostly the same principles, with a different iteration process, is used to allow the use of commercial finite element software within the algorithm, arguably making the model more suitable for use in practice. In addition, changes are proposed to account for radiation between boundary surfaces in the decay phase after the thick fire plume disappears and to include the energy of char oxidation in the presence of high oxygen contents during the decay phase.

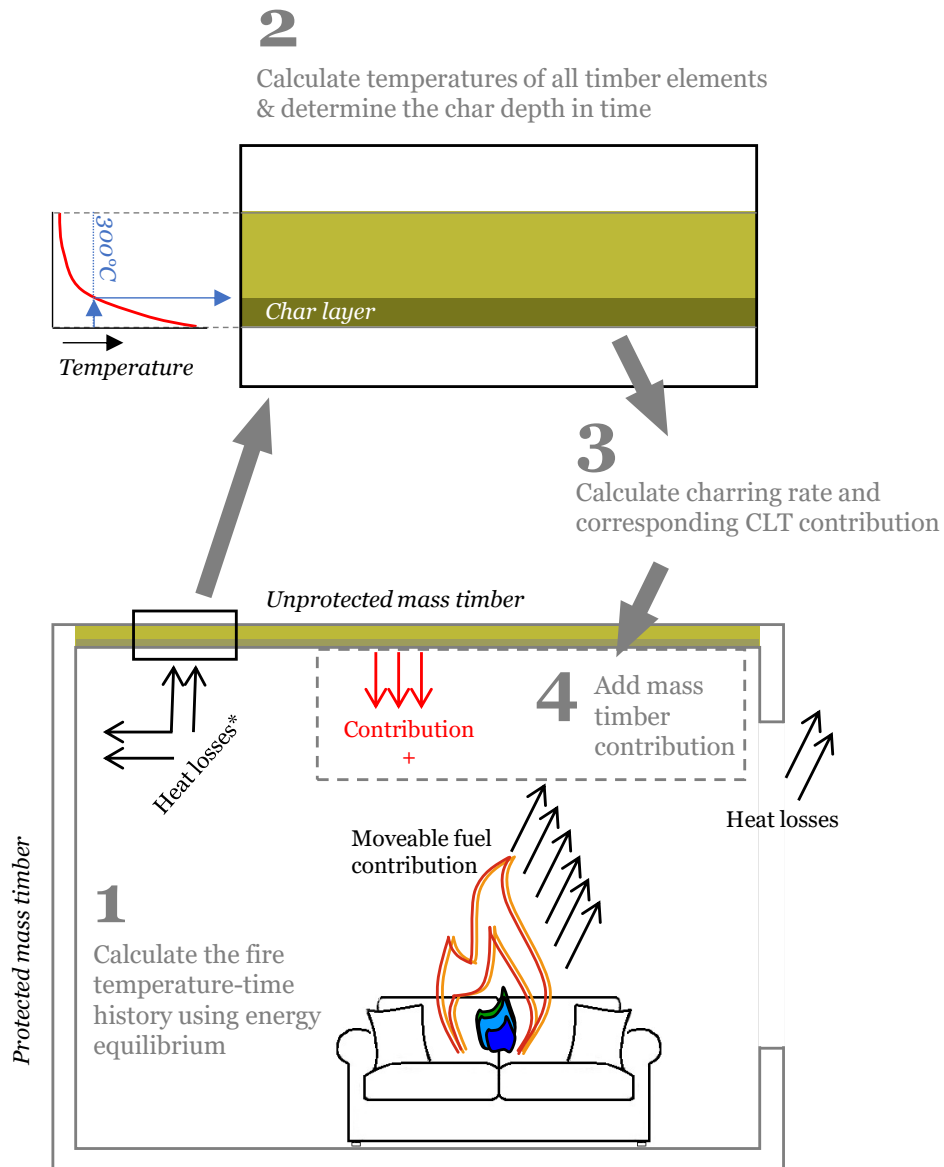
2 The model

2.1 Overview

The model by Brandon and Andersson (2018) and the updated model described within this report are based on the same principles and basic steps, which are illustrated in Figure 1 and schematically in Figure 2, and can be summarised as follows:

1. Calculate the compartment fire temperatures for the full temperature-time history using a single zone model and a heat release rate curve. For the first calculation the heat release rate curve should correspond to the moveable fuel in the room (e.g. the basic fire curve described in Annex B). For all subsequent calculations, the heat release rate curve from step 4 is used.

2. Use these compartment temperatures to calculate the temperature-time history of any protected and unprotected timber structural element.
3. Calculate the charring rate through time for any timber structural element and calculate the potential heat release rate through time due to the charring
4. Add the CLT combustion contribution to contribution of the moveable fuel load.
5. Iterate (i.e. repeat steps 1 to 4) until convergence.



*in the decay phase, the net heat flux is directed from the boundary surfaces towards the room

Figure 1: The four steps of every iteration

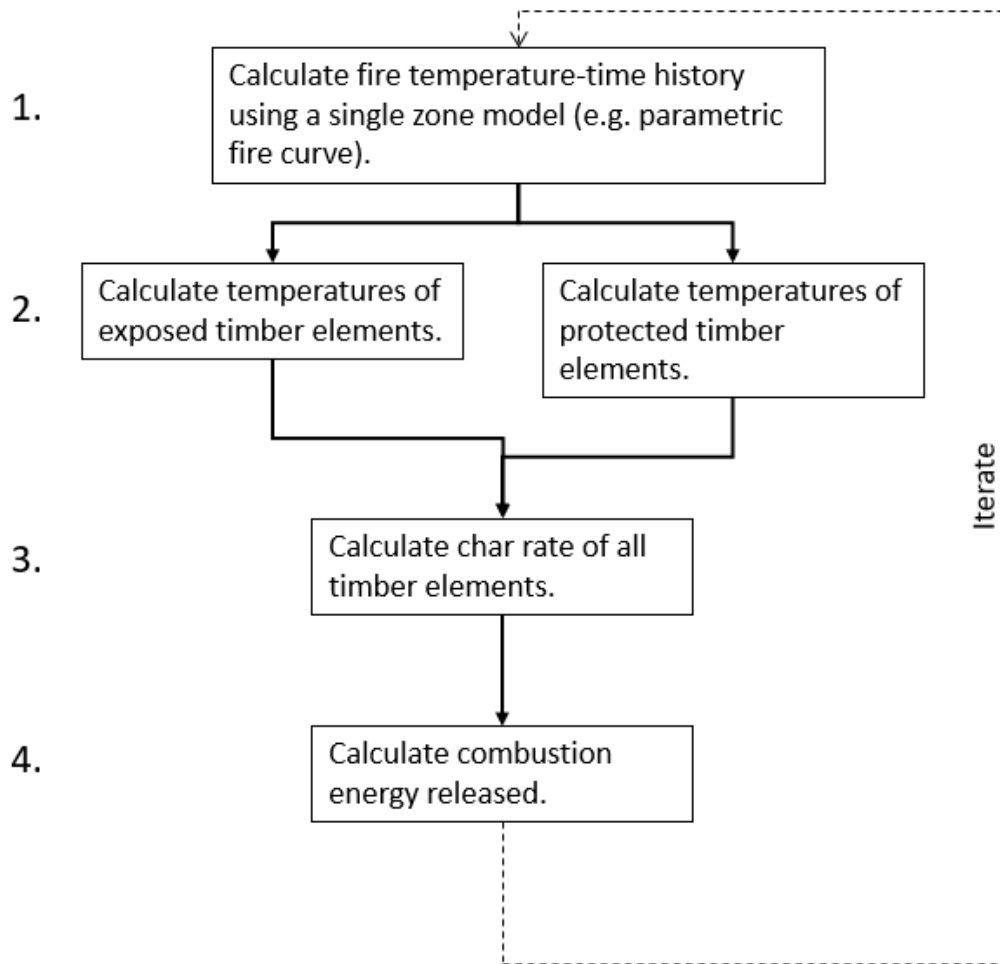


Figure 2: Schematic of model process

The equations utilised for the steps of the model are as developed by Brandon and Andersson (2018) and for the updated model in Annex A. The differences between the previous and updated version of the model are indicated in Section 2.2.

Using the single zone model and knowledge of the heat release rate of the moveable fuel (furniture etc.), initial estimates of temperatures within the room are determined. In addition to the assumptions generally made using single-zone models (e.g. a well-mixed state), the model method involves the assumption that the combustible gasses released as a result of the heating of timber, combust at or near the moment they are released. If there is not enough available oxygen to allow combustion inside the compartment, this combustion will occur outside of the compartment. In the updated model, a portion of the energy is stored in the char layer at the surface to be released in a period with increased access to oxygen to represent oxidation of this char layer. If there is oxygen left inside the compartment, this combustion will take place inside the compartment.

In step 2 the charring of all timber is considered. This includes the protected timber, which can char behind the fire protection if the fire duration is significantly long. Fall-off of the base layer of fire protection can lead to a significant increase of

charring/combustion rate. If a compartment has a combination of protected and unprotected surfaces, or a combination of surfaces with varying protection, the model requires multiple heat transfer calculations to determine the temperature development and charring rate for all varying assemblies to determine their contribution to the fire as a fuel.

Using experimental relationships between charring and heat release rates of timber (Schmid *et al.* 2018) the potential contribution of timber to the fire as a fuel is determined (Step 3) and added to the moveable fuel load (Step 4) as illustrated in Figure 3. The addition of the heat release contribution of timber can increase both the duration of the fully developed phase and/or the fire temperatures.

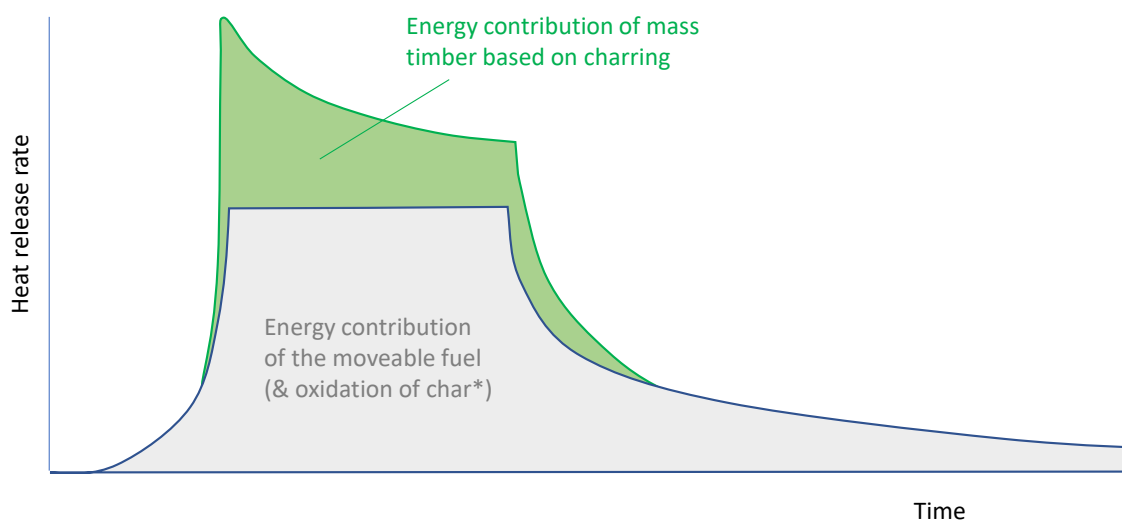


Figure 3: The addition of the energy contribution of mass timber to the input heat release curve.

Because the fire temperature-time history is dependent on the energy contribution of the mass timber and the energy contribution of the mass timber is dependent on the fire temperatures, solving requires a numerical approach. An iterative procedure is implemented (Figure 2) which should converge to a scenario where the energy equilibrium corresponds to the fire temperatures.

With knowledge of the through-depth temperatures of all mass timber members, structural calculations can be performed using relationships between temperature and the structural properties of wood which is studied by numerous authors and included in design standards such as EN 1995-1-2 (2004).

2.2 Model Changes

There have been a number of changes to the model and its implementation when compared to that described previously by Brandon and Andersson (2018). Firstly, in implementation, the heat transfer calculations (required for step 2) are now conducted within a commercial finite element software (SAFIR) to increase the ease of automation

of the process. This means that the calculation of aspects such as the energy losses from the fire into the compartment walls happen once per-iteration for the full time-history, rather than simultaneously with the fire temperature calculation at each timestep (Figure 4). This does increase the number of iterations required for convergence in comparison to the previous implementation. However, the increased ease of automation has improved the speed to run the model for any particular scenario.

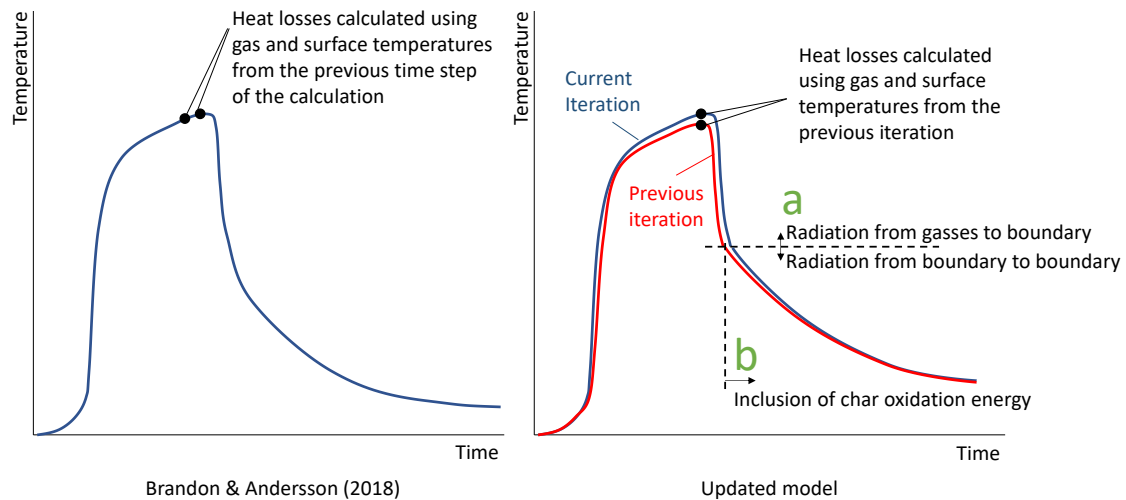


Figure 4: Three differences between the model by Brandon and Andersson (2018) and the updated model. Iterative heat calculations, radiation exchange and inclusion of char oxidation.

More significantly, two changes have been made to the model itself. These are:

- a. Removal of radiation transfer from the gas to the interior surfaces, starting at the stage at which the thick fire plume decays.
- b. A part of the mass timber combustion energy is stored in the char, representing the energy of the char layer which does not oxidize in oxygen poor environments. The combustion due to oxidation of this char takes place during the decay phase.

Both of these changes had an influence in the decay phase, as schematically indicated in Figure 4.

Change “a” is made to more accurately reflect conditions after the thick fire plume has decayed. In this situation the hot gases are no longer opaque, and allow radiative heat to pass through them, rather than providing a radiative surface itself. Radiative losses from each of the hot compartment surfaces (roof, windows, floors) are, therefore, now primarily to each other with a portion to the ambient environment or external surfaces visible through the openings. When considering the whole compartment as a single system, the proportion of heat losses from radiation through the openings will be small for most compartments (with the exception modern fully glazed office buildings). During the fully developed phase much of the radiation emitted by the wall and ceiling surfaces is absorbed by the exiting gasses and direct radiation from these surfaces out of the compartment is mostly absent. In the decay phase it is conservatively assumed that the heat losses remain absent, which is considered reasonable for compartments with limited ventilation openings such as most residential compartments.

At each stage of the iteration, the fuel load is increased to represent the portion of the char which oxidises after the fuel within the compartment is starting to burn out (i.e. when the fire becomes fuel controlled again). For the *a priori* predictions of Chapter 4 this was undertaken only at the final iteration, by including this fuel as an addition to the moveable fuel load in the calculation and there was no cumulative impact of this fuel increase. Attempts including the cumulative impact extended the fully developed phase every iteration and resulted in significantly extended, and unrealistic, flashover periods. This approach assumed that the vast majority of the char oxidation energy would be released in a few minutes after onset of decay of the moveable fuel combustion which is not in line with observations of the char regression in recent tests by Brandon et al. 2021¹. Change “b” maintains the link between the length of flashover/the onset of decay with the moveable fuel load, but includes the energy of oxidation in the period of high oxygen concentration² (Figure 5).

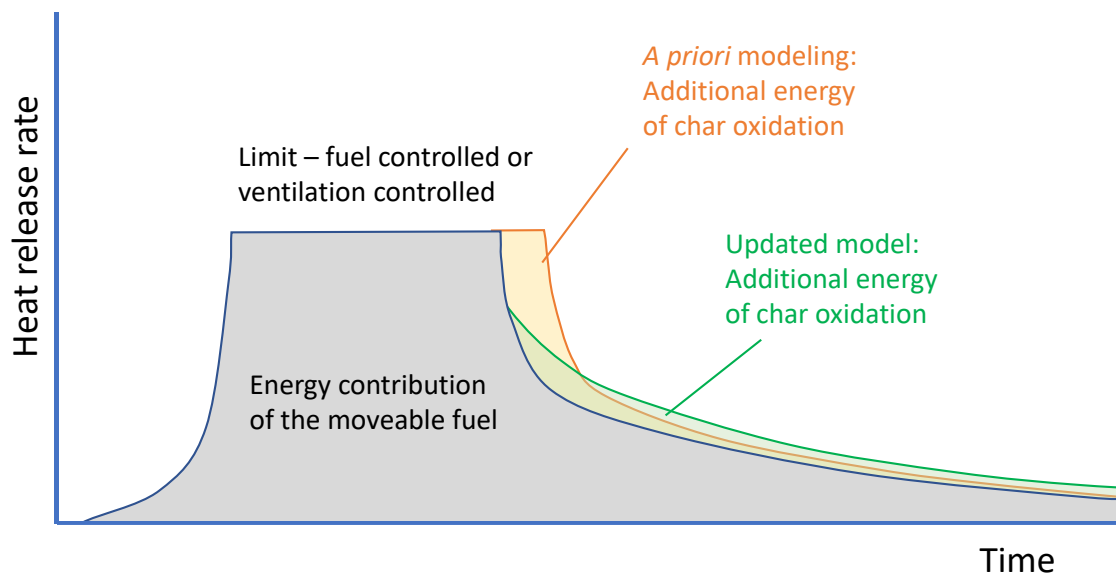


Figure 5: Schematic representation of “change b” mentioned in the main text, where the addition of energy by char oxidation is included in the decay phase after onset of decay of the combustion of moveable fuel only.

¹ The char regression from videos of Test 3 (Brandon et al. 2021) suggest that in the location with the most significant char oxidation, more than 50% of char oxidation took place more than 25 minutes after the switch from oxygen poor to oxygen rich environment. This is based on the change of direction of visible lamellas, which indicates an average rate of char regression per lamella.

² Oxygen measurements presented by Brandon et al. 2021 indicated a sudden switch from oxygen poor to oxygen rich environments at the moment of extinction of flaming combustion in the majority of the compartment. Therefore, extinction of flaming combustion has been used as the criterion for initiating char oxidation in the model.

3 Experiments for comparisons

Comparison of the model was made to the five compartment fire experiments conducted recently in the project *Fire Safe implementation of visible mass timber in tall buildings*. Full details of the experiments can be found in *RISE Report 2021:40* (Brandon et al. 2021). The compartments used within the experiments had internal dimensions of 7.0 m x 6.85 m x 2.73 m. Four of these compartments had two ventilation openings of 2.25 m x 1.78 m (width x height). The remaining compartment test had six larger openings with a total area of 30.2 m². A summary of the key parameters required for each experiment can be seen in Table 1. Additionally, the following fuel and combustion parameters are assumed for all tests, based on Annex B and previous experience of a priori predictions:

- Fuel load density: 560 MJ/m² (target of experiments)
- Heat release rate density: 220 kW/m²
- Fraction of fuel used at start of decay: 0.6
- Fire growth rate: 0.047 kW/s²
- Combustion efficiency: 0.8

Table 1: Summary of key experimental compartment parameters

Test	Opening Area (m ²)	Opening Heights (m)	Exposed Timber Area (m ²)	Gypsum Layers*
1	8.0	1.78	53.8	2
2	8.0	1.78	91.2	3
3	8.0	1.78	96.2	3
4	30.2	2.04	77.9	2
5	8.0	1.78	97.2	3

* Each gypsum layer is 5/8 inch (15.9 mm) thick Type X fire resistive gypsum boards.

4 *A priori* modelling predictions according to Brandon and Andersson

This chapter compares *a priori* modelling predictions made using the model by Brandon and Anderson (2018) recent experimental results and assesses where the model could be improved. This assessment is used as a basis for improvement of the method as discussed in subsequent chapters.

The models presented by Brandon (2016) and Brandon and Andersson (2018) or slight deviations of these models were previously used to predict the heat release rates and temperatures of 14 compartment fire tests prior to the tests and distributed to the respective project reference group and/or visitors of the test on site. These compartment tests were 6 tests by Su et al. (2018); 1 test by Brandon et al. (2018) 3 tests by Zelinka et al. (2018) and 4 tests by Brandon et al. (2020). It should be noted that no attempt was made to equip the model to account for CLT fire induced delamination (or glue line integrity failure). Instead, it is recommended to avoid fire delamination through the utilization of delamination-resistant products or by preventing failure temperatures to be reached in the bond lines. The most relevant comparisons are, therefore, with tests where fire delamination did not occur.

This chapter discusses comparisons between predictions made with the method by Brandon and Anderson and recent full-scale fire test results by Brandon et al. (2021). One alteration was made to the model to account for oxidation of the charred timber once the intensity of the combustion rate of the furniture is lowered, which was indicated before in Section 2.2, Figure 5.

For a full explanation of the model by Brandon and Anderson (2018), the reader is referred to the original report. The purpose of this chapter is to demonstrate the accuracy of the method and to identify possible points of improvement. An updated model is discussed later in this report and explained in detail in Annex A.

Comparisons of the *a priori* modelling predictions and experimental Heat Release Rate (HRR), internal gas temperatures (approximated by thermocouple trees), plate thermometer temperatures and gypsum surface temperatures for Test 2 of the recent test series are shown in Figure 6 and Figure 7.

Similar *a priori* modelling predictions were made for Test 1, 3 and 5 and are shown in Annex C. No *a priori* predictions were made for Test 4 as it was expected that there would be no well-mixed fire conditions in a heavily fuel controlled fire, which is the fundamental assumption of the single zone model.

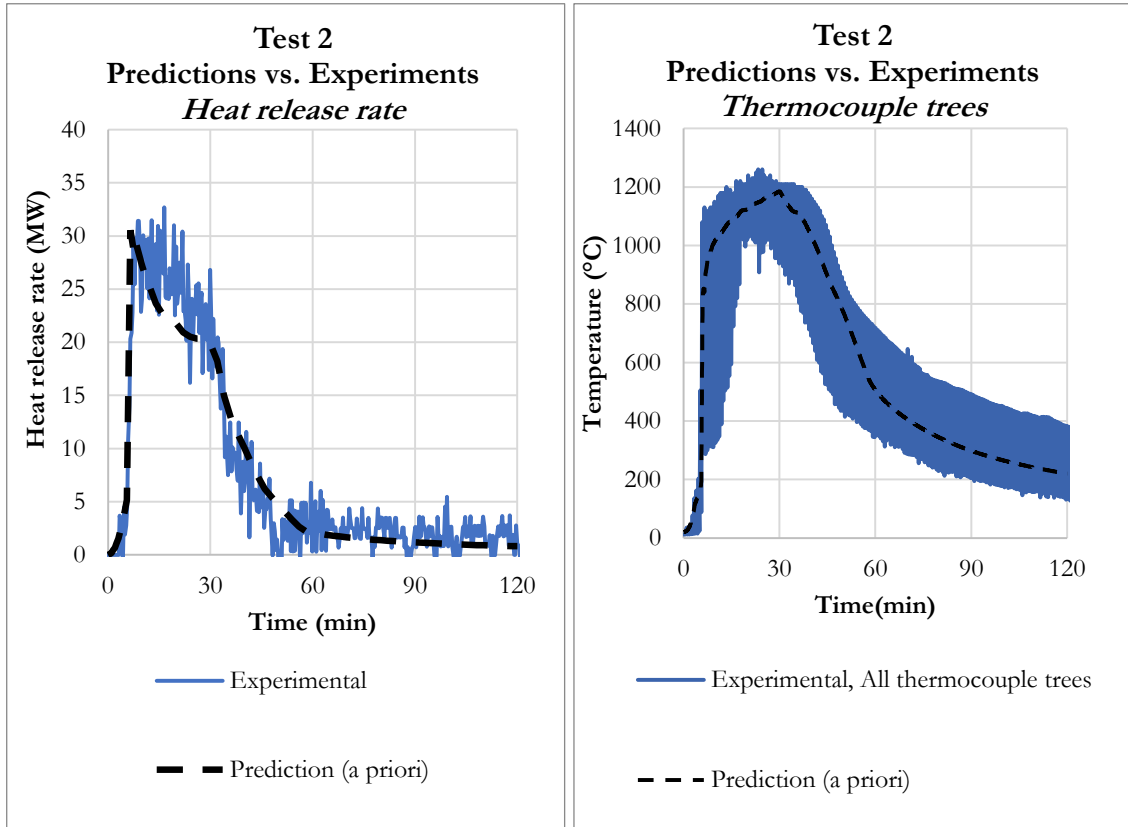


Figure 6: Test 2, predicted heat release set against the experimental heat release rate (left) and predicted fire temperature set against thermocouple tree measurements (right).

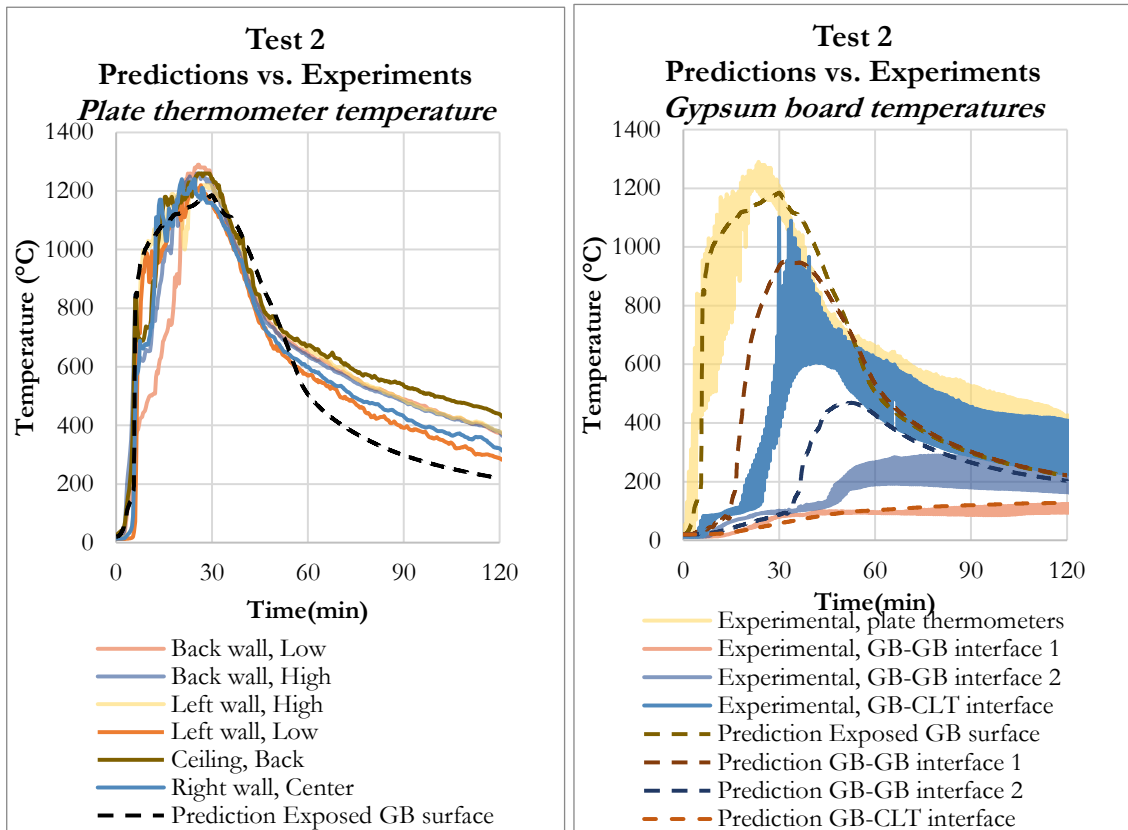


Figure 7: Test 2, predicted fire temperature set against plate thermometer measurements (left) and predicted and experimental temperatures at gypsum board interfaces (right).

The model utilised for *a priori* modelling showed good predictions of peak temperatures, peak duration and of the HRR. It does, however, show a significant underestimation of the temperatures within the decay phase, particularly the later part, as visible in all the temperature comparison plots. The underestimation in temperatures in the decay phase, was less significant for Test 1 with only an exposed mass timber ceiling.

It is proposed that the primary reason for this underestimation in temperatures is due to an overestimation in radiative losses of the compartment. The model assumes that radiative heat transfer between the walls and the gas with a view factor of 1. While this is considered a good approximation during the “flashover” stage of the fire, where the room is filled with dense smoke and opaque flames, it is not as good after the flaming has reduced during the decay phase. At this point the walls will be able to “see” other surfaces (no longer blocked by flames and smoke) and will radiate to the surfaces visible. As the internal walls all have similar temperatures (in a single zone model), radiation between these surfaces simply keeps the energy within the compartment system. Losses via radiation from the system are only to what can be seen through any openings. Other than for Test 4 all of the compartments considered have a total opening area that is small in comparison to the overall internal surface area of the compartment and as a result the portion of radiation which is lost from the compartment through openings is small after flaming stops. Figure 8 gives a 2-dimensional illustration, indicating the portion of radiation going out of the rooms considering a location in the back of the compartment. In 3-dimensional space the share of radiation exiting the compartment is significantly less.

Another inconsistency between the *a priori* modelling and the experimental work concerns the implementation of char oxidation. In these *a priori* predictions the char oxidation was assumed to mostly occur directly after the moment the moveable fuel combustion starts to decay. This is however not in line with the experimental measurements, as the oxygen concentration in that period of the fire was still close to zero in most locations.

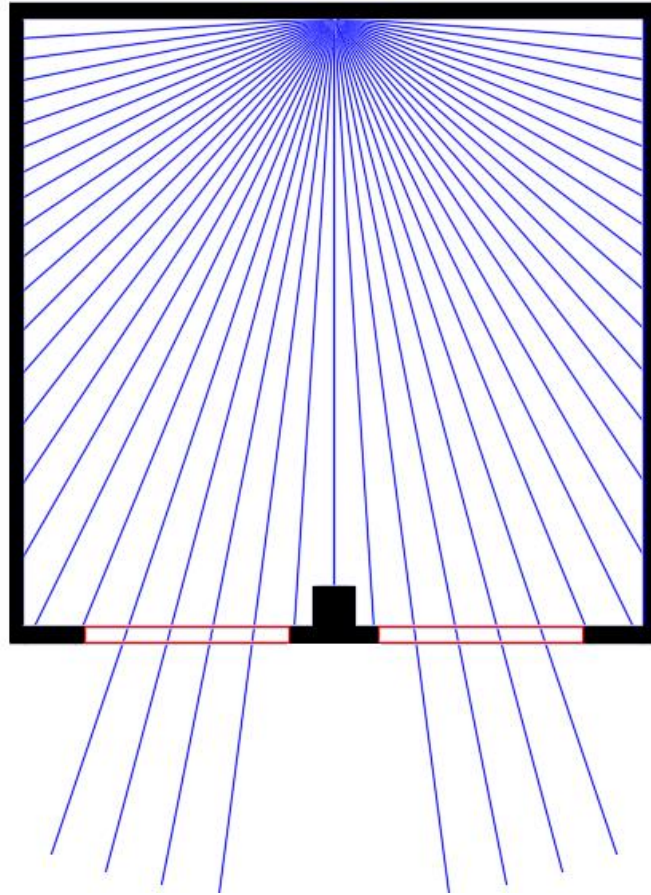


Figure 8: Illustrative example of the relative portion of radiation passing through the compartment openings. Note: in 3-dimensional space the relative portion is significantly smaller than apparent in this figure.

5 Updated model of this study

As discussed in Section 2.2 the updated model that has been further developed is based on the same basic building blocks, with improvements (removal of radiative losses from the walls in the decay phase and inclusion of the energy by char oxidation) and an updated implementation (utilising Matlab and SAFIR to increase automation of the process). The updated implementation also included a further change, whereby the energy from the oxidation of the char in the later stages of the fire as it transitions back into the fuel-controlled regime is added, thereby adjusting the slope of the decay. All calculation steps of the updated model are described in Annex A.

Side by side comparison of the plate thermometer temperatures of Test 2 and the predicted surface temperature of gypsum boards are given on the left side of Figure 9. The measured and predicted temperatures behind each layer are set against each other on the right side of this figure.

For the entire fire duration an improved correspondence between predicted surface temperatures and measured plate temperatures was seen. As the surfaces of both, the plate thermometer and the gypsum board are relatively thermally inert and their temperatures are dominated by thermal radiation, this comparison indicates the

predicted and thermal radiation interaction was improved in the updated model. Until a late stage of the decay phase thermal radiation accounts for the vast majority of heat transfer into (and out of) the surfaces, while the convective heat flux is relatively insignificant. This comparison indicates therefore that the predicted thermal exposure to the compartment boundary corresponds well with the experiments.

Figure 10 indicates a slight underestimation of temperatures in the decay phase of Test 3, which had exposed walls intersecting in corners. From analysis of the test data, it was concluded that a radiative feedback loop in the bottom of the corners between combustible walls had a significant effect in the decay phase (Brandon et al, 2021). The low locations this occurred at, in the compartment, corresponded to regions where the measured oxygen concentration was relatively high already during the fully developed phase of the fire. This indicates the lower parts of the exposed corners had an environment in which significant char-oxidation would take place. The radiative feedback loop would occur especially between surfaces that experience relatively high rates of char oxidation, with a high view factor relative to each other. The zone model is not equipped to perform such local analysis and the implementation of vertical elements with relatively high view factors is not recommended without further analysis.

The prediction of temperatures behind gypsum board layers seems to be on the conservative side (Figure 9, right), especially deeper in the specimen. It is expected that the use of more suitable thermal properties for the gypsum material can increase the accuracy.

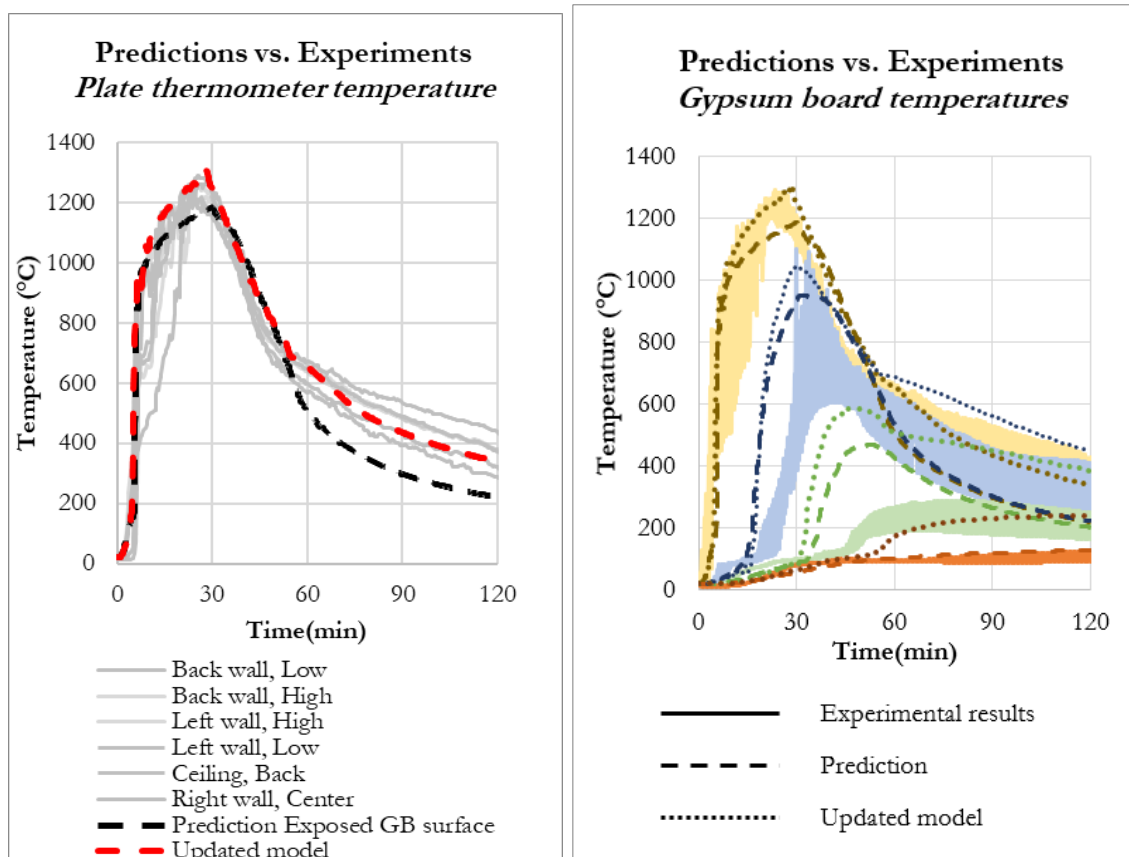


Figure 9: Comparison of both model versions against experimental results (plate thermometers and gypsum interfaces).

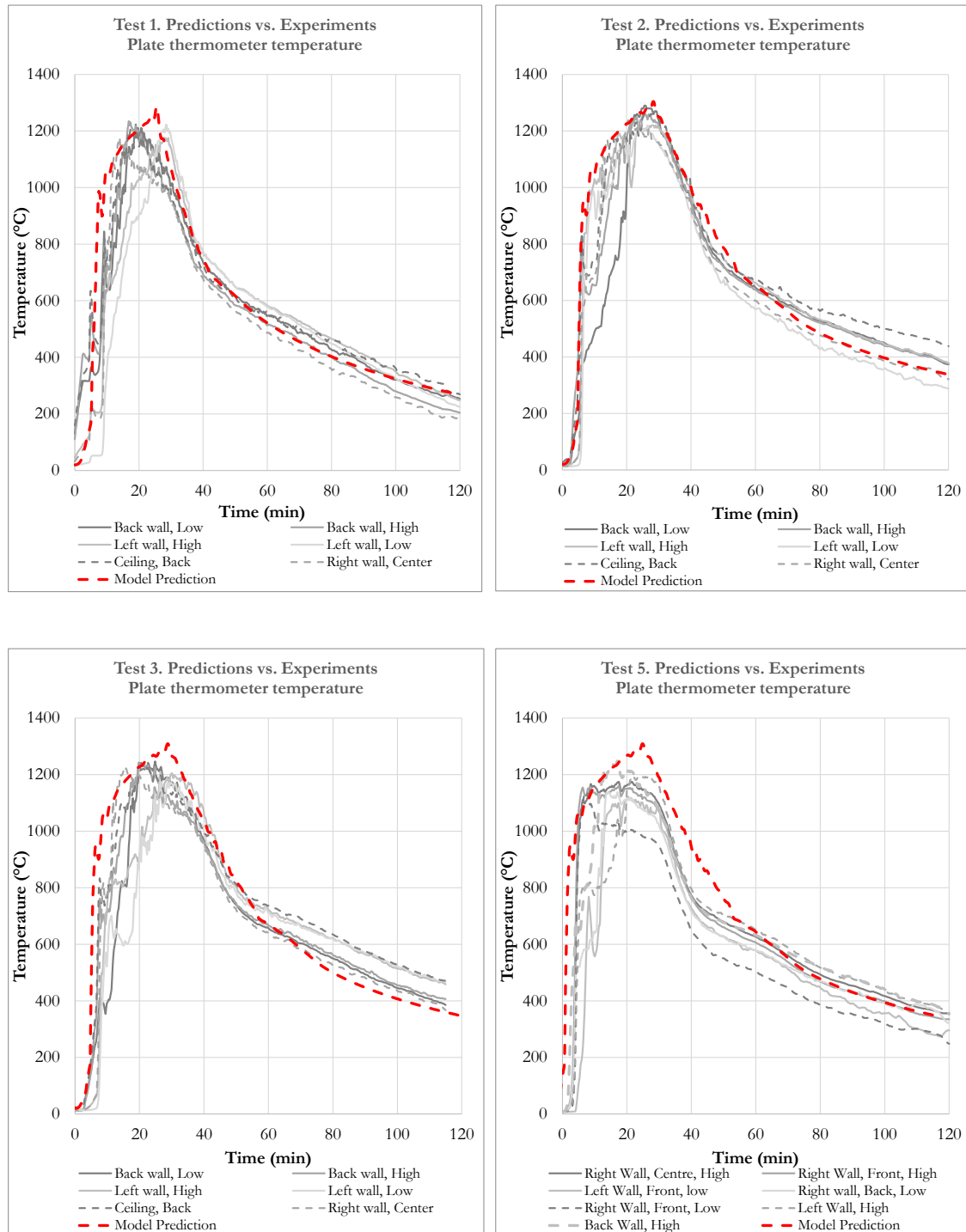


Figure 10: Comparison of model results from the "updated model" vs the experimentally measured surface temperatures for tests 1, 2, 3 and 5.

Comparisons between the experimental heat release rate (determined from mass loss rates) and both a priori and updated predictions are shown in Figure 11 (left). Comparisons between the gas temperatures and the thermocouple tree temperatures are shown on the right side of the figure.

In comparison with the model of the *a priori* predictions, the updated model predicts a slightly lower heat release rate (HRR), as a larger part of the combustion energy is stored for char oxidation. For the *a priori* predictions it was assumed that char oxidation can take place also in the fully developed phase, as long as it fitted within the stoichiometric limit of the compartment. Although there were signs of relatively local char oxidation already in a part of the fully developed phase, experimental oxygen measurements indicated that the majority of the surfaces only were exposed to high oxygen concentrations after the extinction of flames. For the updated model, it was therefore assumed that all char-oxidation would take place after the extinction criterion for flaming combustion was reached (which was chosen as a fire temperature of 700°C for this study). As a result of this, the predicted HRR drops earlier than the *a priori* HRR predictions. The total heat of the fire appears to be slightly underestimated as the area under the predicted heat release rate curve seems to be smaller than the area under the experimental curve. Although local char oxidation (in locations with an oxygen rich environment already during the fully developed phase) would increase the predicted heat release of the updated model, there are some other possible explanations for the difference between the calculated and experimental heat release rate. It is expected that a combination of these factors also plays a role:

- Possible slight underestimation of the heat release rate contribution of charring wood.
- The lower part of the compartment is charring more than predicted and underestimation of the average char depth would lead to an underestimation of the average heat release rate.

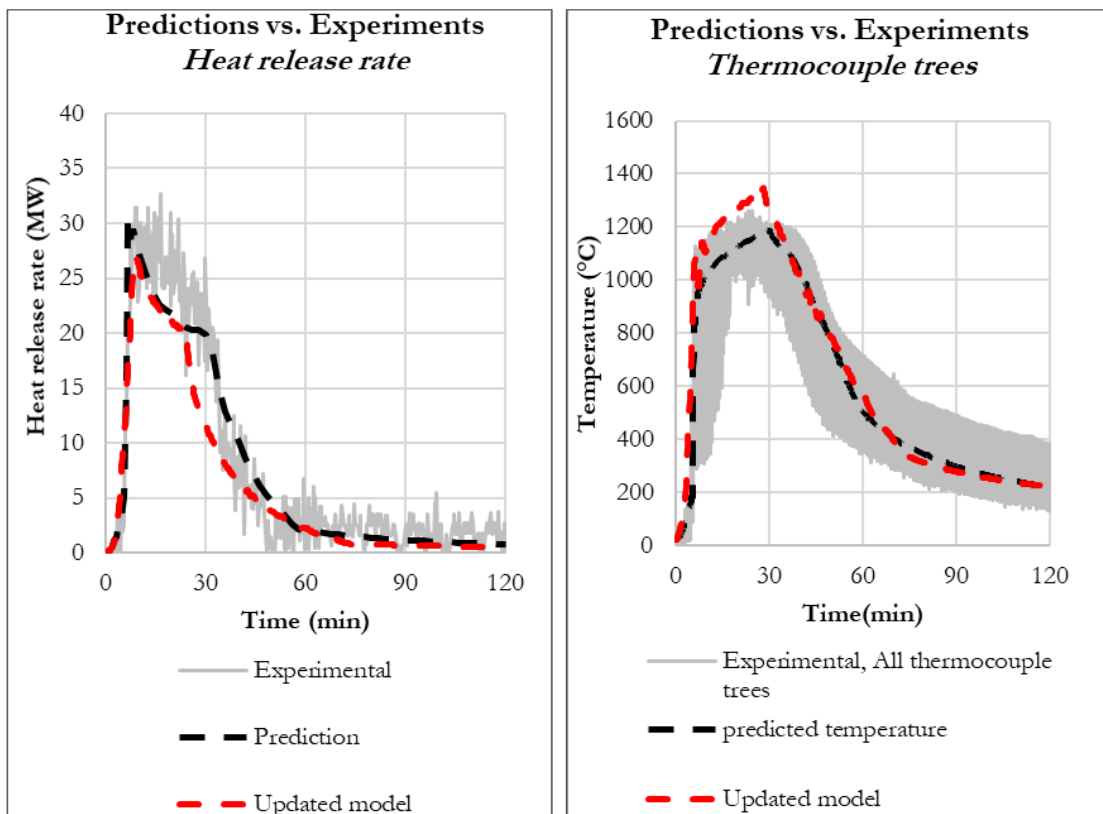


Figure 11: Comparison of both model versions against experimental results.

The predicted heat release rates using the updated model are set against the experimental heat release rates in Figure 12.

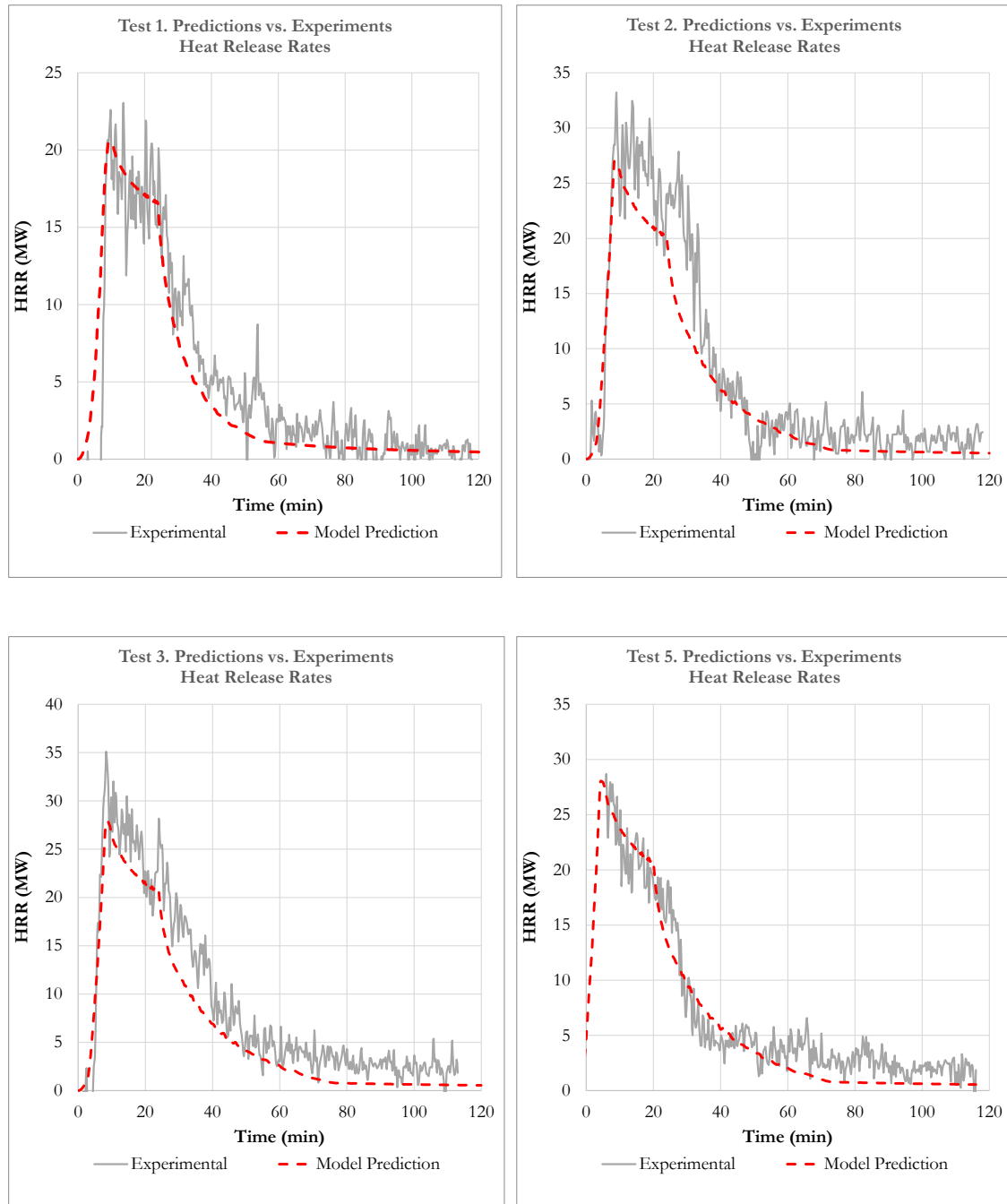


Figure 12: Comparison of model results from the "updated model" vs the experimentally calculated HRR for tests 1, 2, 3 and 5. *Note: There were technical issues with the logging of load cells at the start of Test 5 so there is no experimental HRR for the first ~10 minutes see report by Brandon et al. (2021) for further details*

The gas temperatures seem to be overestimated in the fully developed phase (using the temperatures from thin thermocouples as a proxy for gas temperature). For the decay phase the predicted gas temperatures fall within the lower part of the temperature range

measured in Test 2, 3 and 5 and within the higher part of the temperature range of Test 1. The gas temperature predictions are not as accurate as the surface temperature predictions. However, for accurately predicting the heat transfer into the compartment boundaries, the accuracy of gas temperature predictions is however of far less importance than the accuracy of the predicted radiation conditions.

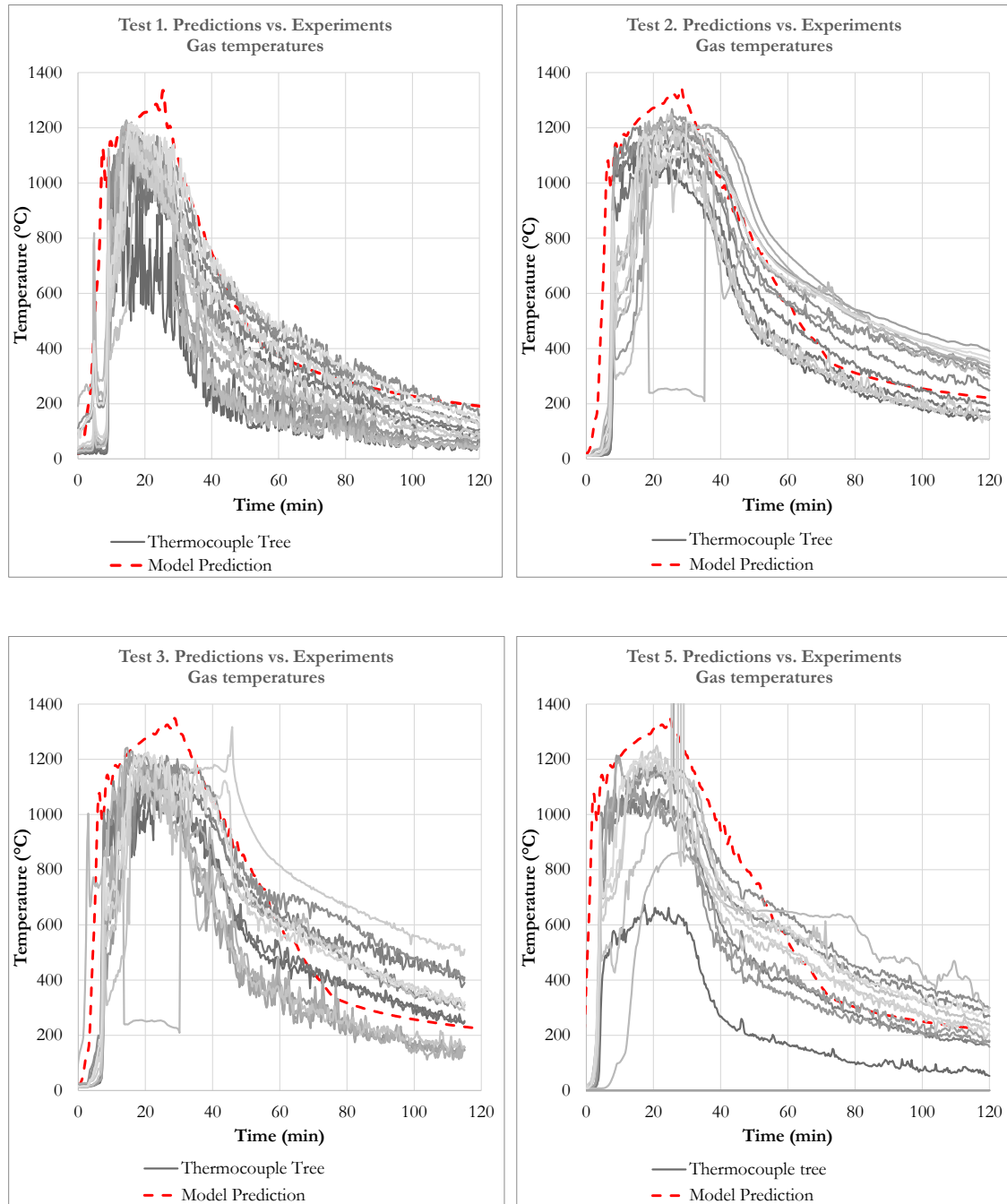


Figure 13: Comparison of model results from the "updated model" vs the experimentally measured gas temperatures for tests 1, 2, 3 and 5.

The measured char depths after the tests varied significantly with location within the experimental study, with the lowest level of charring found on the ceiling and the highest levels generally at the foot of the walls, especially in fully exposed corners. It is expected that this is caused, in part, by the variation in oxygen concentrations across the compartment (see report by Brandon et al. (2021) for more details) which in addition to any special variation of conditions is a phenomenon which is not considered within the model. If it is assumed that timber chars at temperatures above 300°C (Buchanan and Abu, 2017) the char depth predicted by the model can be compared to those measured in the experiments. The char depths for both the models and experiments are shown in Figure 14 and Figure 15. The char depths after the full fire duration calculated by the model are, with the exception of Test 4 (discussed later), all within the bounds of the char depths measured from the tests. Generally, the predicted char depth is around the mean of wall char depths and above the maximum char depths recorded on the ceiling. This indicates that the predicted char depths are likely to be above the average char depth.

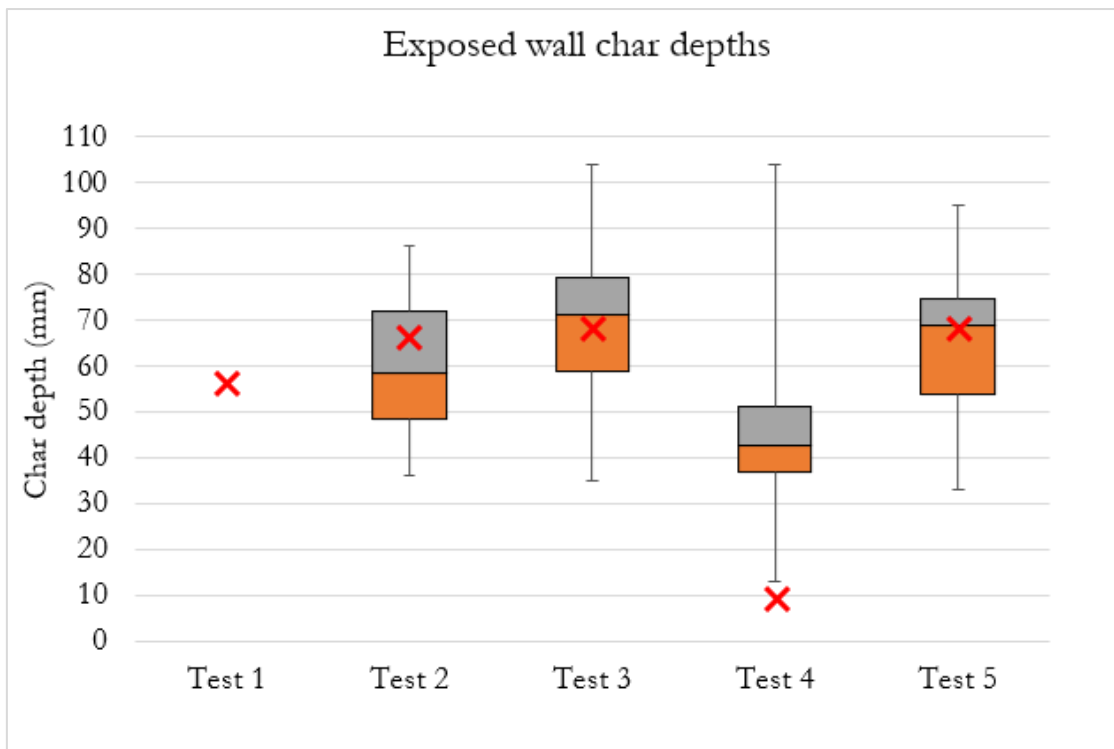


Figure 14: Char depth distributions as measured from experimental data on exposed wall surfaces with depths predicted from the model (red crosses). No walls (only ceiling) were exposed in Test 1.

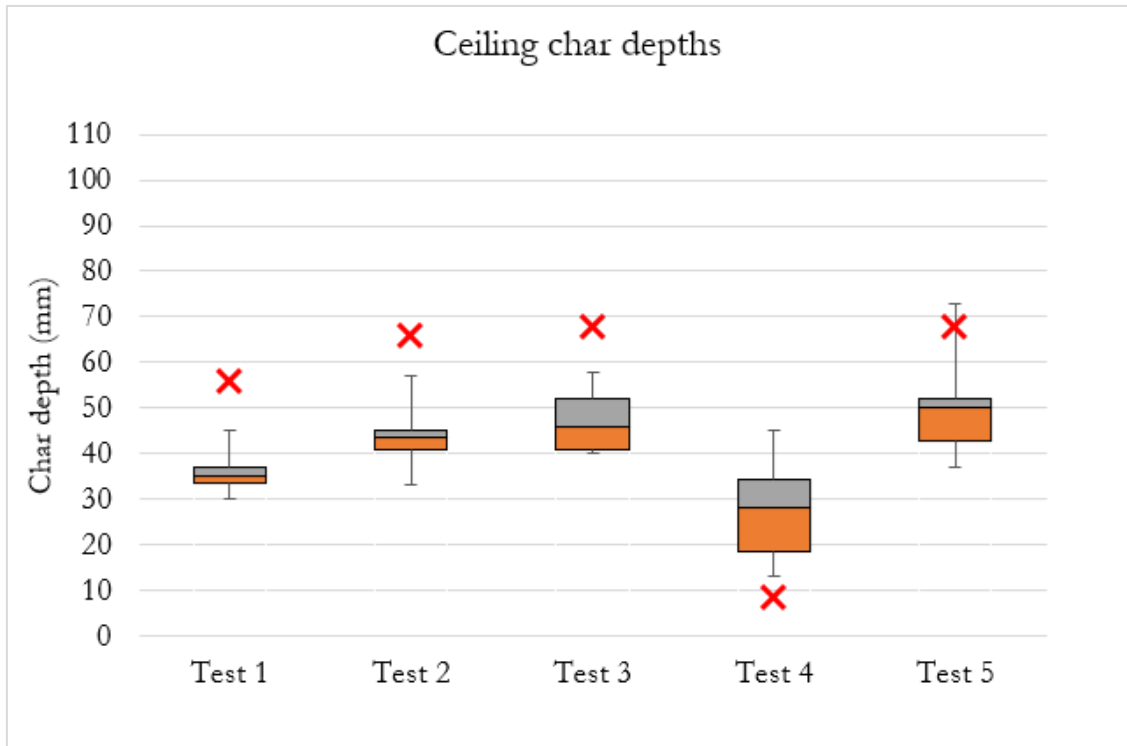


Figure 15: Char depth distributions as measured from experimental data on the exposed ceiling surfaces with depths predicted from the model (red crosses).

5.1 Test 4 - large opening predictions

Test 4 had much larger openings (and opening factor) than the other tests. This leads to two things: firstly, the assumption that the compartment is in a well-mixed state may no longer be valid; and secondly, that the basic fire curve utilised (which was determined from compartments with a range of smaller opening factors) in implementation of this model underestimates fires in these conditions. This underestimation is related to large heat convective losses from the compartment, which when combined with the relatively small fire assumed gives low gas temperatures and minimal charring. This low level of charring subsequently does not provide sufficient extra heat release to increase the fire temperatures and duration. In Test 4, the oxygen flow was provided from three sides as three facades had large openings. It is expected that significantly larger front of high oxygen concentration led to a faster burn rate of the moveable fuel that was experienced in compartments with significantly smaller opening factors.

To assess this hypothesis (that the majority of the underestimation is in the assumed fire from the movable fuel load) the HRR calculated from the mass loss of only the movable fire load in the test is used as an input to the model in place of the basic fire curve. This was determined from mass loss measurements of the floor which excluded the mass loss of the rest of the structure. See the project *Final Report* by Brandon et al. (2021) for full details on how this HRR is calculated. For this comparison, no implementation of the elongation of the fire by char oxidation after the peak has been made where the HRR from the tests has been used.

Comparisons between the model results for Test 4 with the basic fire curve and the experimental fire curve for the movable fuel as inputs against the experimental results can be seen in Figure 16.

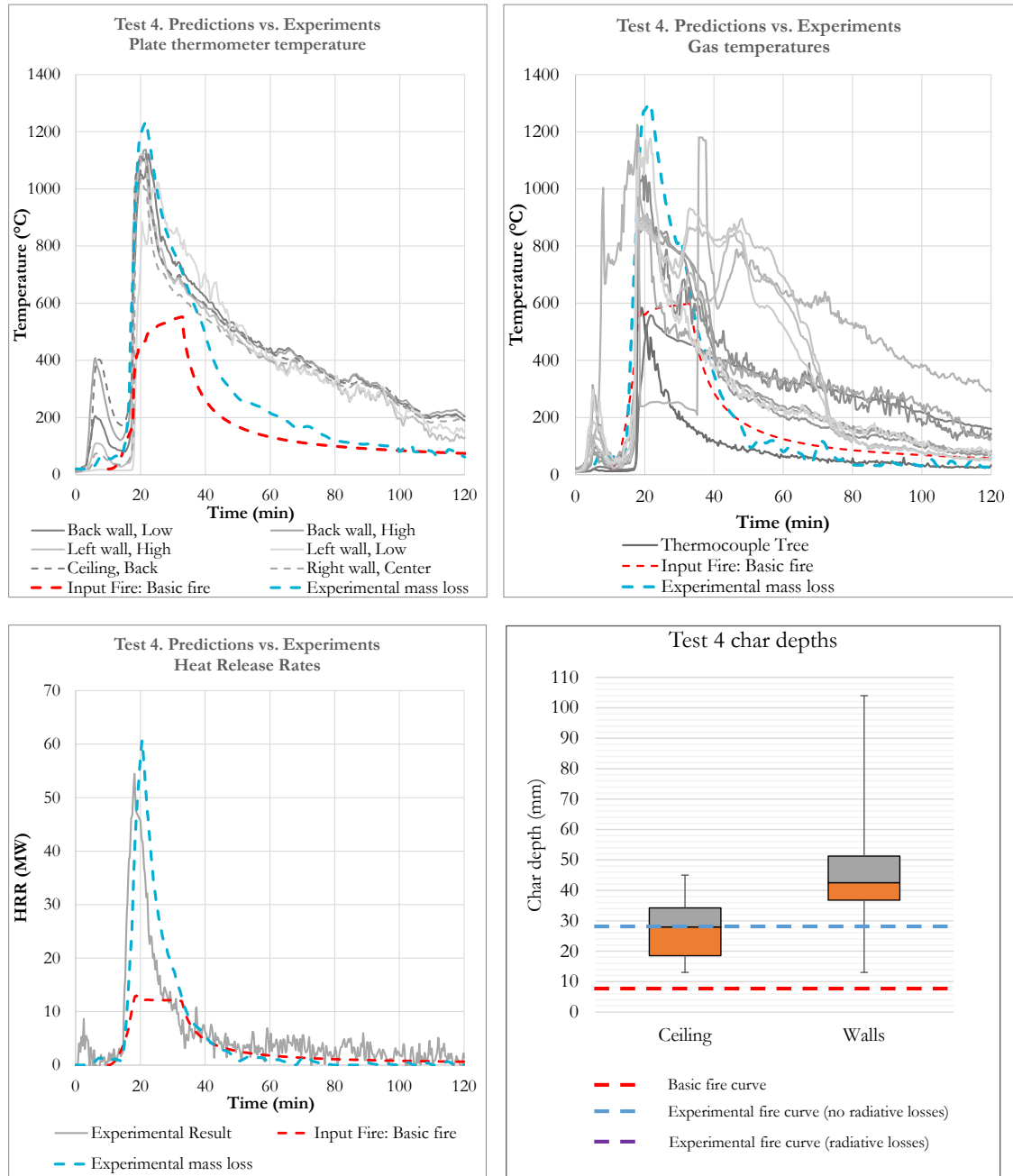


Figure 16: Modelling results comparing the difference where the HRR calculated from experimental mass loss rate (i.e. movable fuel load only) is utilised as the input HRR curve for Test 4.

The model results, when the experimental HRR of the movable fuel load is used, provide a good match to the real results in terms of peak temperatures, both gas and surface, and the duration of this peak. They also provide significantly better estimations of the char depth for the ceiling. However, the prediction of the char depth of the walls was still low, below the 2nd quartile for the walls. There is a notable underestimation in the

temperatures during the decay phase after 40 minutes, and an underestimation in the total HRR from a similar point. There are three probable causes of this:

- Prior to input into the model the HRR for the burning of the movable fuel from the experiment was smoothed, during the later stages of the fire there continued to be some HRR measured, but this was very noisy and the smoothing reduced this part to almost 0. Glowing embers were observed during the later stages of the experiment and it is likely that the HRR curve used for the model underestimated the contribution of the moveable fuel during this period.
- An underestimation of the radiative feedback loop between surfaces, as discussed in relation to the modelling of the other tests. This is particularly relevant at corners of two exposed walls where re-radiation between the exposed surfaces leads to an increased level of charring.
- Char oxidation and increased char at the bottom of the compartment overall has likely led to a slower decay. As mentioned, for the calculations of this section, extension of hot phase by char oxidation was not included.

5.2 Areas for further improvements

Through the implementation of the updated model a number of areas for further improvement, both within the model itself and its implementation, have been identified:

- Improved set of gypsum material properties. The through-depth temperatures of the gypsum boards, particularly at greater depths later in the fire, are significantly over-predicted. An improved set of gypsum material properties would give better indication with regards to the risk of charring behind the gypsum.
- Inclusion of combustion energy on the protected side of gypsum boards if protected mass timber starts charring. In the models of this report all heat release takes place inside the compartment, while it in reality is possible that at least a part of the heat is released behind fire protective layers, which prolongs the effect of charring behind gypsum boards.
- Implementation of a progressive gypsum falloff model. Where attempts at modelling gypsum falloff have been undertaken with the current implementation the falloff occurs in a single instant. This leads to a sudden exposure of a large area of cold surface to the fire, a big spike in energy losses, and a set of discontinuities in compartment temperatures (as well as a significant overestimation in any charring behind the gypsum) and as a result is currently only used as an indication of risk of falloff. Where gypsum falloff actually occurs in real scenarios, it happens in fits and starts with small areas of gypsum falling off over time. Implementation of a progressive model would allow for a more accurate representation of this. Any practical implementation would require either 3D heat transfer calculations of conduction through the gypsum and timber, or a larger number of 2D models for capturing the gradient in temperatures within the gypsum and timber around areas where the local falloff occurs at different times.
- Implementation of higher surface temperatures of exposed timber due to char oxidation. In the decay phase of real scale compartment fire tests, the difference between the surface temperature of combustible walls and gypsum protected walls was more significant than predicted. This is explained by the location of the

combustion during the decay phase. Having these surfaces in close vicinity in locations where a high rate of char contraction was observed (caused by char oxidation) has led to local radiative feedback loops, prolonging the exposure. It is recommended that these locations are avoided until there is a method to accurately predict this interaction.

- Improve implementation for custom/alternative variable fuel load HRR curves. The current implementation is mainly set around the basic fire HRR curve as described in Annex B. While this curve appears to work well for compartments with normal fuels (i.e. a mix of cellulosic and plastic fuels as typically found in most residential and office spaces) in relatively low ventilated spaces, it does not necessarily work for fires outside of these constraints (as demonstrated with the initial results for Test 4). Improved implementation for the use and generation of alternative HRR curves for the movable fuel load would allow for an increased scope of application.

In addition to improvements of the model calculations. Further experimental studies are recommended to expand the knowledge of:

- Heat release rate distribution of char oxidation in the decay phase.
- Scenarios where a significant radiative feedback loop between combustible surfaces slows down or prevents decay.
- Further experimental work to determine the relationship between charring and heat release rates.

6 Conclusions

A single-zone model used for *a priori* predictions of a series of compartment fire tests was set against the experimental results after completion of the tests. This comparison indicated a good correlation of the predicted and experimental heat release rates and fire temperatures during the fully developed phase. However, in the decay phase, the *a priori* model systematically underestimates the temperatures. It was expected that the method of including the energy of char oxidation in the decay phase and the presence of radiative interaction between the gasses and the surface for the full duration of the decay phase were the reasons for these underestimations.

An updated version of the model was developed, which, has (1) an updated method for the inclusion of char oxidation energy and (2) a simulated shift from radiative interaction between surfaces and gasses to an interaction between surfaces after the disappearance of fire plumes. In addition, the model uses commercial software, SAFIR, for through-depth temperature calculations, reducing the total calculation time and arguably increasing the practicability.

Predicted surface/ plate temperatures using the updated model correspond better with experimental results than the *a priori* predictions for the whole fire duration. The changed radiative interaction has increased these temperatures in the decay phase, which corresponds better with the experimental results.

The predicted char depths after the full fire corresponded roughly to the average measured in exposed CLT walls of compartments with opening dimensions that correspond to residential occupancy (Brandon 2021) and the char depth of the ceiling

was overestimated. The final char depth in the bottom of walls was, however, generally underestimated. This underestimation is most significant at the foot of corners where two exposed CLT walls intersect.

The heat release rates and the total heat released was slightly underestimated for some tests. This is likely partially due to an underestimation of charring and char oxidation in the foot of exposed walls and exposed wall corners.

The updated model requires a suitable combustion rate curve for the moveable fuel content of the compartment as input. Empirical relationships describing such curves are given in Annex B. However, it should be noted that these relationships were determined from a range of compartment designs and that extrapolation out of this range is not always suitable. For predictions of a fire in a relatively open compartment, heat release rate of the moveable fuel was significantly underestimated using the relationships of Annex B. Using the experimentally determined combustion rate of the moveable fuel instead of the relationships of Annex B led to a significant improvement of predictions.

References

- APA—The Engineered Wood Association. (2017). ANSI A190.1-2017: Standard for Wood Products-Structural Glued Laminated Timber.
- APA—The Engineered Wood Association. (2018). ANSI/APA PRG 320: 2018: Standard for performance-rated cross-laminated timber. American National Standard. Tacoma, WA: APA-The Engineered Wood Association, 246.
- Barber, D., Crielaard, R., & Li, X. (2016, August). Towards fire safe design of exposed timber in tall timber buildings. In World Conference on Timber Engineering (wcte2016), Wien, Austria.
- Brandon, D. (2016). Practical method to determine the contribution of structural timber to the rate of heat release and fire temperature of post-flashover compartment fires.
- Brandon, D. (2018). Fire Safety Challenges of Tall Wood Buildings—Phase 2: Task 4-Engineering methods. National Fire Protection Association. NFPA report: FPRF-2018-04.
- Brandon, D., & Anderson, J. (2018). Wind effect on internal and external compartment fire exposure. RISE Research Institutes of Sweden.
- Brandon, D., Sjöström, J., Hallberg, E., Temple A., Kahl, F. (2021) Fire Safe implementation of visible mass timber in tall buildings – compartment fire testing. RISE Report 2021:40. Research Institutes of Sweden, Borås, Sweden.
- Buchanan, A. H., & Abu, A. K. (2017). Structural design for fire safety. John Wiley & Sons.
- Chen Z. (2008). *Design fires for motels and hotels*. Master thesis. Department of Civil and Environmental Engineering Carleton University. Ottawa-Carleton Institute of Civil and Environmental Engineering, Ottawa, Ontario, Canada.
- EN 1991-1-2 (2002) - Eurocode 1: Actions on structures - Part 1-2: General actions - Actions on structures exposed to fire. CEN standards.
- EN 1995-1-2 (2004) - Eurocode 5: Design of timber structures - Part 1-2: General - Structural fire design. CEN standards.
- Hopkin D, Anastasov S, Brandon D (2017) Reviewing the veracity of a zone model based approach for the assessment of enclosures formed of exposed CLT. In *Applications of Fire Engineering*. CRC Press/Balkema, the Netherlands.
- Janssens, M., Huczek, J., & Albracht, N. (2016). Performance of Gypsum-Protected CLT and NLT in Natural and Standard Fires. Structures in Fire.
- Li, X., Zhang, X., Hadjisophocleous, G., & McGregor, C. (2015). Experimental study of combustible and non-combustible construction in a natural fire. *Fire Technology*, 51(6), 1447-1474.
- Magnusson S.E. and Thelandersson S. (1970) Temperature – Time Curves of Complete Process of Fire Development. *Acta Polytechnica Scandinavica, Civil Engineering and Building Construction Series 65*, Stockholm, Sweden.

- McGregor, C.J. (2013) Contribution of cross-laminated timber panels to room fires. Master thesis. Department of Civil and Environmental Engineering Carleton University. Ottawa-Carleton Institute of Civil and Environmental Engineering, Ottawa, Ontario, Canada.
- Rockett J.A. (1976) Fire Induced Gas Flow in an Enclosure. *Comb. Sci. and Tech*, 12: pp 165-175
- Schmid, J., Santomaso, A., Brandon, D., Wickström, U., & Frangi, A. (2018). Timber under real fire conditions—the influence of oxygen content and gas velocity on the charring behavior. *Journal of Structural Fire Engineering*.
- Schmid, J., & Frangi, A. (2021). Structural Timber In Compartment Fires—The Timber Charring And Heat Storage Model. *Open Engineering*, 11(1), 435-452.
- Staffansson L. (2010) *Selecting Design Fires*. Lund University Report 7032, Sweden.
- Su J., Lafrance P-S., Hoehler M., Bundy M. (2018) Cross Laminated Timber Compartment Fire Tests for Research on Fire Safety Challenges of Tall Wood Buildings – Phase 2.
- Su J.Z. and Lougheed G.D. (2014) *Report to research consortium for wood and wood hybrid mid-rise buildings – Fire safety summary – Fire research conducted for the project on mid-rise wood construction*. National Research Council Canada, Client report: A1-004377.1, Ottawa, Ontario, Canada.
- Wade, C., Hopkin, D., Spearpoint, M., Su, J., & Fleischmann, C. (2019). Enclosure fire model for mass timber construction—benchmarking with a kinetic wood pyrolysis submodel. In *Interflam: 15th International Conference on Fire Safety Engineering* (pp. 1-3).
- Wickström, U. (1986). A very simple method for estimating temperature in fire exposed concrete structures.
- Wickström U. (2016) *Temperature calculation in Fire Safety Engineering*. Springer International Publishing, Switzerland.
- Zelinka, S. L., Hasburgh, L. E., Bourne, K. J., Tucholski, D. R., Ouellette, J. P., Kochkin, V., & Lebow, S. T. (2018). Compartment fire testing of a two-story mass timber building. United States Department of Agriculture, Forest Service, Forest Products Laboratory.

Annex A: Updated Single Zone Model

A.1: Step 1 – Calculate fire temperature time history using an equilibrium approach

Step 1 of each iteration indicated in Section 2.1 uses a single zone model to determine the gas temperature. Knowledge of the heat release rate corresponding to the movable fuel load, \dot{Q}_C is required as input for the calculation. Empirical relationships allowing to do this are proposed in Annex B. It should be noted that these relationships are determined from compartments with typical residential furnishing and opening factors ranging from 0.031 to 0.084 m^{0.5}.

The model discussed in this Annex uses a combination of (1) the input heat release of the moveable fuel, \dot{Q}_C and (2) the heat release rate corresponding to mass timber, $\dot{Q}_{C;CLT}$ to calculate the fire temperatures using a single zone model that is based on energy equilibrium. $\dot{Q}_{C;CLT}$ is determined from the charring rate (step 3 as discussed in Section 2.1), which is predicted using a heat transfer model (step 2). The heat transfer model is also used to determine the heat loss through the CLT compartment boundaries, which is needed for the single zone model (step 1), as discussed below.

The law of conservation of energy states that there is an equilibrium of energy. The energy released should, therefore, be equal to the energy lost (hereby the heat energy stored in gasses inside the compartment is considered negligible):

$$\dot{Q}_C + \dot{Q}_{C;CLT} = \dot{Q}_W + \dot{Q}_R + \dot{Q}_L \quad \text{eq. A1}$$

Where:

\dot{Q}_C is the heat release rate corresponding to the movable fuel load

\dot{Q}_W is the rate of heat loss through compartment boundaries (floor, walls and ceiling)

\dot{Q}_L is the rate of heat loss through air flow out of openings in the compartment

\dot{Q}_R is the rate of heat loss through radiation out of openings

$\dot{Q}_{C;CLT}$ is the heat release rate of the CLT calculated using a heat transfer model

The maximum heat loss rate due to air flow out of the openings is determined using (Wickström 1986):

$$\dot{Q}_L = \alpha_1(T_f - T_\infty)cA\sqrt{h} \quad \text{eq. A2}$$

Where:

T_f is the fire temperature (K).

T_∞ is the ambient temperature (K)

c is the specific heat of air

α_1 is a flow rate coefficient

The factor α_1 is a flow rate coefficient and is often assumed to be 0.50 kg/(s m^{5/2}). According to Rockett (1976) the value of this coefficient ranges between 0.40 and 0.61 kg/(s m^{5/2}). In this study the value of α_1 is chosen empirically, using the series of post-flashover fire tests of compartments with non-combustible linings shown in Table B.1.

As shown in Annex B, a value of $\alpha_1=0.40$ corresponds well with these experimental results.

Until the flame extinguishment criterion³ is reached one single fire temperature is assumed, which is considered reasonable for thick flames where radiative heat transfer takes place between the compartment boundary surfaces and the combusting gasses. After the extinction of flames the compartment boundary surfaces would radiate to each other and the gas temperature decreases faster than the radiation temperature. In the model the temperatures of the gypsum surface and the CLT surface are very similar throughout the whole fire. In addition, view factors of all compartment boundaries to each other are often close to unity for residential compartments (except if opening surface areas are very large. For the period after flame extinction, it is for simplicity assumed that there is zero net heat flux between the compartment boundaries, which corresponds to a compartment in which all surfaces have the same temperature and a view factor of 1.0 between all compartment boundaries. For the model of this report this is done numerically, by reducing the surface emissivity to zero. The radiative heat transfer from the compartment boundaries to the gasses, (only included in the period of flaming combustion) is calculated as follows (Magnusson and Thelandersson, 1970):

$$\dot{Q}_{R,CP} = \sigma \varepsilon (T_f^4 - T_s^4) \quad \text{eq. A3}$$

Where:

σ is the Stefan Boltzmann constant

ε is the effective emissivity

T_s is the surface temperature

For practical purposes, some assumptions had to be made regarding radiation through the openings. To indicate the influence of these assumptions, the radiation out of real compartment fires is discussed first.

In a period after flashover, in the presence of a thick interior fire plume, the combusting gasses can radiate heat out of an opening. However, if there is a thick fire plume going out of the opening for a period, this external fire plume can partially block the outgoing radiation. The exiting fire plume will become thinner some time before the start of a decay phase, which reduces this blocking effect. In this report, this effect is ignored, which indicates that the radiative loss in a period after flashover is overestimated.

Already before the flaming combustion stops, a part of the compartment boundary radiates heat through the opening. Including radiation from each compartment boundary to the openings would require a complex and time consuming 3-dimensional numerical analysis and would result in varying surface temperatures throughout the whole compartment. In order to keep the calculation pragmatic and affordable, it is assumed that the gasses radiate out of the compartment opening instead with a view factor of 1.0. After the fire plume disappears in the decay phase, the walls will directly radiate heat out of the openings. The view factor of all boundary surfaces to the opening is 1.0 for compartments with all openings in the same plane (where they do not have radiative interaction). However, to keep the model pragmatic, this change of radiation source is not included in the model. As the gas temperatures are lower than the surface

³ which is around 600 to 700°C and corresponds roughly to 33 to 51 kW/m²

temperatures of the compartment boundary during the decay phase, this should conservatively lead to an underestimation of the heat losses.

Using the above assumptions, the radiative heat loss through the opening is included using:

$$\dot{Q}_{R,CB} = A_O(T_f^4 - T_\infty^4)\sigma \quad \text{eq. A4}$$

Where:

A_O is the surface area of all openings

For compartments with relatively small openings in multiple façade it can still be reasonable to assume a view factor of 1.0 or close to 1.0. For compartments with large openings in multiple facades, it is recommended to either adjust implement a reduced view factor of surfaces towards openings, or conservatively ignore the radiative heat loss after extinction of flaming combustion entirely.

The heat loss rate through the CLT boundaries, \dot{Q}_W , is calculated using the heat transfer model, discussed in the next section.

The single zone model uses a simple algorithm to solve the fire temperatures. The fire temperature is determined by substituting eq. A2 into eq. A1 and solving to determine T_f (Brandon, 2016):

$$T_f = \frac{\dot{Q}_C + \dot{Q}_{C,CLT} - \dot{Q}_W - \dot{Q}_R}{c\alpha_1 A \sqrt{h}} + T_\infty \quad \text{eq. A5}$$

The fire temperature is calculated from the heat losses using eq. A5. However, the calculation of the heat losses requires knowledge of the fire temperature. Therefore, this problem cannot be solved purely analytically and requires a numerical procedure, which is done differently by the models of Brandon and Anderson (2018) and the updated model of this report. As indicated in Figure 17, the model by Brandon and Anderson calculates the fire temperature from the heat losses of the previous time step. By reducing the size of the time step the error reduces. The model proposed in this report uses the heat losses of the previous iterations to calculate fire temperatures of the current iteration. This method requires some measures in the first few iterations to ensure convergence. In the first iteration the contribution of mass timber is taken as $\dot{Q}_{C,CLT} = 0$ and the heat losses through walls and radiation through openings are assumed to be half of the heat release rate, because information from the previous iteration does not exist. This assumption will be corrected by subsequent iterations. Once the model output of subsequent iterations is not changing significantly, the iterative procedure is stopped. The model of the current report requires significantly more iterations than the previous model. However, it allows the inclusion of commercially developed finite element software to calculate the timber temperatures, this makes it a more viable option for practical use.

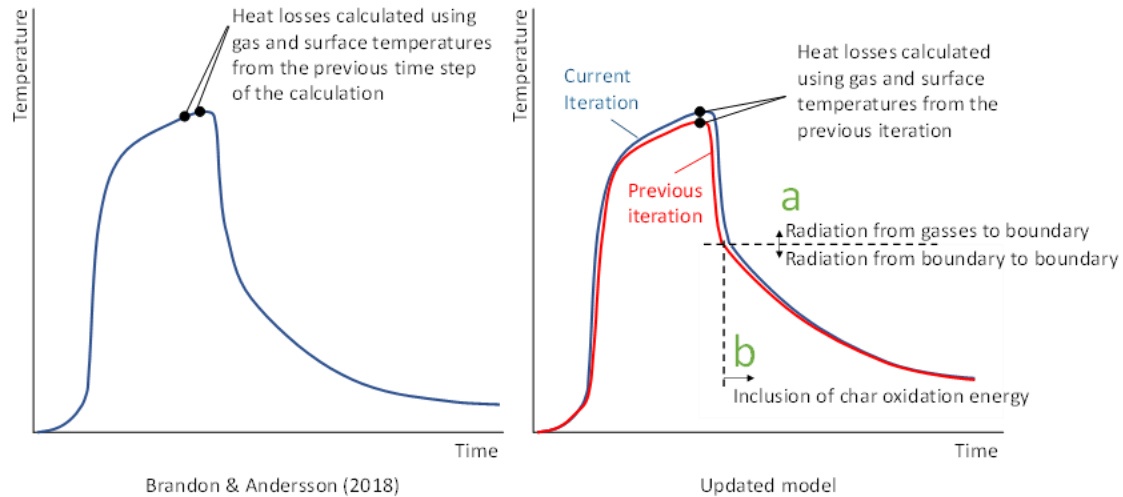


Figure 17: Three differences between the updated model and the model by Brandon and Andersson (2018)

A.2: Step 2 – Calculate temperatures of all timber members

The calculation of the contribution of CLT, glued laminated timber or other mass timber materials $\dot{Q}_{C,CLT}$ is determined using a 1-dimensional⁴ finite element heat transfer model to predict the heat transfer from the exposed side of the wall to the unexposed side. On both sides the following boundary condition is assumed to account for convection and radiation:

$$q_n = h(T_f - T_s) + \sigma\varepsilon(T_f^4 - T_s^4) \quad \text{eq. A5}$$

Where:

q_n is the net heat flux through the surface,
 h is a convection coefficient (W/m²K),

The used convection coefficient and emissivity are 25 W/m²K and 0.8, respectively, which are in accordance with EN 1991-1-2 (2002) and EN 1995-1-2 (2004).

In the presence of a thick fire plume the gas and radiation temperature are very similar and a single fire temperature is used for the expression of temperature. Once the flaming combustion extinguishes and the surface flaming disappears, the effective thermal radiation interaction is mostly between compartment boundaries for compartments and through the ventilation openings. In a compartment with only exposed CLT members and gypsum protected members the surface temperatures of the boundaries are fairly

⁴It should be noted that compartments with a significant amount of mass timber members of small dimensions, exposed from multiple sides, may require a 2-dimensional heat transfer model for accurate representation.

similar according to the model predictions. The net radiative heat flux between these surfaces is, therefore, close to zero, unless the compartment has very large openings. This is simulated in the model by reducing the emissivity of the walls to zero after the auto-extinction of flaming combustion⁵ for the calculation of heat transfer through the walls. In this report the auto-extinction fire temperature of flaming combustion of 700°C was used. This corresponds to incident radiant heat flux of approximately 51 kW/m², which is on the high end of the range for flame extinction criteria found in the literature. A relatively high value was chosen as already before surface flaming completely stops the surfaces become visible to each other.

Heat transfer/ temperature calculations should be performed for all wall and floor assemblies with different built-ups, including those that have gypsum board protection. The heat transfer calculations are performed for two reasons:

1. determine the total heat loss through the compartment walls, floor and ceiling;
2. determine the heat release rate of the CLT from the charring rate, which is determined from the temperature development in the mass timber.

The total heat loss through wall, floor and ceiling assemblies is calculated using:

$$\dot{Q}_w = \sum_{i=1}^m \dot{q}_{n,i} * A_i \quad \text{eq. A6}$$

Where:

$\dot{q}_{n,i}$ is the net heat flux per surface area through assembly i

A_i is the surface area of assembly i

m is the number of assemblies

The effective thermal properties of timber and the gypsum board used are shown in Table 2 and Table 3. The thermal properties for temperatures in-between the temperature values of the table were linearly interpolated. Care was taken to choose a suitable element size and size of the time steps for the calculations.

⁵ While this is not a physically accurate representation of what happens, the mathematical effect (of making the heat transfer between the gas and walls via radiation equal to 0) is the same.

Table 2: Effective thermal properties of CLT material implemented for predictions made for the main report

Temperature (°C)	Conductivity (W/mK)	Specific Heat (J/kgK)	Density (kg/m ³)
20	0.07	1347	494.6
98	0.06	987	494.6
99	0.73	4006	494.6
120	0.75	6075	494.6
121	0.20	2577	494.6
200	0.67	2300	494.6
250	0.82	3671	460
300	0.24	1936	375.9
350	0.12	4305	257.2
400	0.14	3388	187.9
500	0.15	4472	163.2
600	0.53	7799	138.5
800	0.82	9192	128.6
1220	1.37	9192	1

Table 3: Effective thermal properties of gypsum boards implemented for predictions made for the main report

Temperature (°C)	Conductivity (W/mK)	Specific Heat (J/kgK)	Density (kg/m ³)
20	0.40	960	896
70	0.40	960	896
100	0.27	960	896
130	0.13	14900	829.7
140	0.13	25200	808.2
150	0.13	21700	785.8
170	0.13	960	741.9
600	0.13	960	741
720	0.33	4360	740.1
750	0.38	960	695.3
1000	0.80	960	695.3
1200	2.37	960	695.3

A.3: Step 3– Calculate the charring rate and the corresponding mass timber contribution

Using the char temperature of wood of 300°C (Buchanan and Abu, 2017; EN1995-1-2:2004), the charring rate during the whole fire can be estimated from the calculated timber temperatures. Results of previous studies (Schmid *et al.*, 2018) have shown a constant heat release per millimeter of charring of 5.39 MJ/m²mm. This relationship is hereby used to determine the heat release rate from the calculated charring rate:

$$\dot{Q}_{C;CLT} = \sum_{i=1}^m 5.39 * \frac{\beta_i}{60} * A_i * \alpha_2 \quad (MW) \quad \text{eq. A7}$$

Where:

β_i is the charring rate (mm/min)

A_i is the surface area of assembly i (m²)

α_2 the fraction of combustion energy release in oxygen poor environment

In the decay phase, reduction of the char layer thickness was observed in compartment fire experiments (Brandon et al. 2021), which was a consequence of char oxidation. The oxygen measurements of these experiments suggested that the majority of surfaces were subjected to low oxygen concentration approximately until the extinction of flaming combustion. Results of thermogravimetric analyses (Figure 18) indicate a relatively small and slow reduction of mass in char of temperatures exceeding 400 °C in an oxygen poor environment. In an oxygen rich environment the mass reduces more rapidly and char completely gasifies due to char oxidation. This comparison indicates that a switch from oxygen poor to oxygen rich environment can involve a significant release of additional energy stored in the char layer. Depending on the temperature gradient, the mass fraction of the char layer in comparison to wood is roughly 0.25. The heat release per millimetre of charring of 5.39 MJ/m²mm in equation A7 was determined from cone calorimeter tests in ambient oxygen concentration, where the average charred material has a much smaller mass fraction of the original wood mass. The cone test is used as a basis for the heat release rate prediction, in which the specimen has a small mass fraction of char left. Assuming (1) an average char mass fraction of roughly 0.05 in cone conditions and (2) that wood and char have a similar heat of combustion, leads to a fraction of the combustion energy released (relative to the cone test) in oxygen poor environment of around $\alpha_2 = 1-(0.25-0.05)=0.8$. This value for α_2 is used in this report.

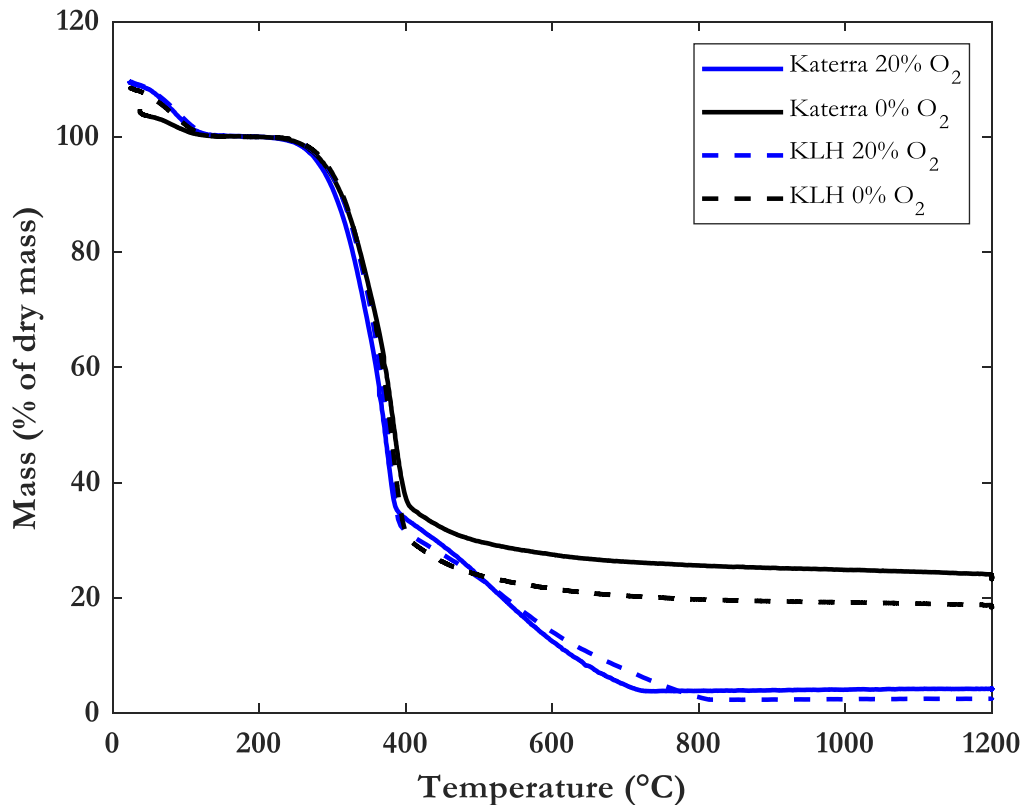


Figure 18: Thermogravimetric analysis results of CLT samples in ambient and nitrogen environment. Heating rate of 20°C/min.

An alternative could be considered, where the mass and mass loss rate is determined from the temperature profile in the mass timber members together with knowledge of the timber density at the relevant range of temperature. The heat release rate (assuming 100% combustion efficiency) would then be calculated using the mass loss rate and the timber material's heat of combustion. This approach would, however, be ignoring the time dependence of the combustion process completely. Although this error could be solved by using Arrhenius equations for calculations of the combustion rate, the added complexity caused by changing oxygen concentrations throughout the fire have been avoided by using experimental relationships instead.

A.4: Step 4– Add the mass timber contribution

The mass timber contribution obtained from equation A7 is added to the heat release rate for the following iteration, by substitution in equation A4 (step 1). However, this does not include the energy of char oxidation which has to be included using another step.

The total energy stored in the char that oxidizes after extinction of flames is:

$$(1 - \alpha_2)\alpha_3 \int_0^{t_{fe}} \dot{Q}_{C;CLT}(t) dt$$

Where t_{fe} is the time at which flame extinction occurs or, alternatively, the time at which oxidation is assumed to start. α_3 is the fraction of the stored char that is actually released due to oxidation. In the current report, no curve fitting is implemented and $\dot{Q}_{C;CLT}$ was not expressed as a function of time. Therefore, numerical integration was implemented in order to determine the stored fuel for oxidation.

Recent experiments (Brandon et al. 2021) indicated that, especially in the ceilings and the top of walls in the compartment, a significant fraction of the char does not oxidize. As a suitable value for α_3 is dependent on the compartment design, the location of the exposed mass timber and the fire scenario, a conservative approach taking $\alpha_3 = 1.0$ is taken in this report.

Although there is some knowledge of when oxidation starts and of the total heat of oxidation, knowledge of the heat release by oxidation is limited. A recent test suggested that char regression caused by oxidation is most significant in the first half hour⁶ after switching from an oxygen poor to oxygen rich environment. Afterwards the char regression slows down.

For the model of this report it was aimed to find a pragmatic solution to include heat energy of oxidizing char. Therefore, the char oxidation energy was added to the heat release rate curve of the moveable fuel load and distributed over the period after flame extinction using the hyperbolic function which was already used to describe the decay phase (see Annex B.5). By using a hyperbolic function, a larger release of heat takes place in the first period and starts to slow down for a long period afterwards. The exact way, the char oxidation energy was included is described in Annex B.5.

In case an alternative heat release time history of the moveable fuel is chosen, the oxidation energy can be included using a separate distribution of the char oxidation heat release over time. Further research to find a suitable distribution is recommended.

⁶ For fire exposed cross laminated timber, an analysis of the direction of the visible lamellas in compartment fire tests can give an indication of char regression, which is a consequence of char oxidation in a high oxygen concentration environment. For the study of the current report a recent test (Test 3 reported by Brandon et al. 2021) was further analysed. A video recording of the left wall showed the directions of visible lamellas and included oxygen measurements at different locations. Locally in the bottom of the wall the oxygen content switched from oxygen poor to oxygen rich in the fully developed phase. 25 minutes after that the surface of the second layer of lamellas became visible in this location. This indicates a char regression of approximately 1.4 mm/min for 25 minutes. About 185 minutes later the third layer became visible at this location, indicating a further char regression of 0.25 mm/min. The analysis therefore indicates more regression and more char oxidation in the hotter phase of the fire. The majority of other oxygen measurements indicated a switch from oxygen poor to oxygen rich environment when surface flaming extinguished. The char oxidation in those locations was significantly less pronounced.

A.5 Iterative procedure

The calculation of the fire temperature, T_f , using eq. A4 requires knowledge of the heat release rate corresponding to the CLT, $\dot{Q}_{C;CLT}$. However, $\dot{Q}_{C;CLT}$ is calculated using T_f . This problem is solved iteratively, starting the first iteration with $\dot{Q}_{C;CLT} = 0$. In the first iteration, the fire temperatures correspond to the heat release rate of the movable fuel load only. The CLT temperatures and charring rates are determined based on those temperatures. The corresponding heat release rate of CLT $\dot{Q}_{C;CLT}$ is used to calculate the fire temperature in the subsequent iteration. This allows the same process and the calculation of $\dot{Q}_{C;CLT}$ for the second and subsequently third calculations and so forth. The iterative procedure is stopped when the change of $\dot{Q}_{C;CLT}$ in subsequent iterations is considered negligible.

Annex B: Defining the movable fuel load fire

The heat release rate (HRR) corresponding to solely the movable fire load (combustible content of the compartment) is required as model input for the single-zone model discussed in Annex A. This information should be based on the fuel type, quantity of fuel and the ventilation condition in the compartment. Examples of methods to generate a suitable heat release rate curve are given by Chen (2008) and Staffansson (2010). The method used in this Annex is based on previous flashover fire tests in non-combustible compartments, with typical apartment furniture as fuel and is discussed here.

B.1 Review of Experimental Data

The heat release rate corresponding to solely the variable fire load is needed as input for the model presented herein. Therefore, it is important that the fire tests used for correlation excluded involvement of combustible structures in the fire. An overview of the compartment fire tests used for this Annex is shown in Table B.1.

Table B.1: overview of compartment tests with non-combustible linings and no sign of combusted construction

Test	Reference	Name in ref.	Floor area of ignited comp. (m ²)	Ventilation opening area of ignited comp. (m ²)	Height of ventilation opening (m)	Opening factor ^v	Main struct.mem-bers ^{vi}	Thickness and type of gypsum board layers (exposed layer last)	Fuel type	Movable fire load density (MJ/m ²)	First item ignited
<i>B2</i> ⁱⁱ	McGregor, 2014	test 2	15.75	2.14	2.00	0.042	CLT	12.7mm fire rated 12.7mm fire rated	furniture	533	bed
<i>B4</i> ⁱⁱ		test 4	15.75	2.14	2.00	0.042	CLT	12.7mm fire rated 12.7mm fire rated	furniture	553	bed
<i>C1</i>	Li <i>et al.</i> , 2014	test 4	15.75	2.14	2.00	0.042	LTF	12.5mm type C 12.5mm type C	furniture	614	bed
<i>C2</i>		test 5	15.75	2.14	2.00	0.042	LTF	12.5mm type C	furniture	610	bed
<i>C3</i>		test 6	15.75	2.14	2.00	0.042	LSF	12.5mm type C	furniture	601	bed
<i>D1</i>	Chen, 2008	test 1	15.72	2.25	1.50	0.040	LSF	12.7mm cement board 15.7mm type X ⁱ	furniture	397	bed
<i>D2</i>		test 2	15.72	2.25	1.50	0.040	LSF	12.7mm cement board 15.7mm type X ⁱ	furniture	366	bed
<i>E1</i>	Su and Loughheed, 2014	LSF	52.54	4.50	1.50	0.031	LSF	12.7mm, 15.9mm type X or standard	furniture	550 ⁱⁱⁱ	bed
<i>F1</i>	Janssens 2016	test 1	14.80	3.87	2.07	0.084	CLT & NLT	type X ^X type X	furniture	575 ^{iv}	sofa
<i>F2</i>		test 2	14.80	3.87	2.07	0.084	CLT	type X ^X type X	furniture	600 ^{iv}	sofa

ⁱ two layers of 15.9mm type X gypsum board on the ceiling

ⁱⁱ also reported by Li *et al.* ⁹

ⁱⁱⁱ movable fire load density:

- bedroom 510 MJ/m²;
- living area 380 MJ/m²
- kitchen dining area 970 MJ/m²
- average living/dining/kitchen 575 MJ/m²
- whole apartment average 550 MJ/m²

^{iv} rough estimation using graph in resource

^v opening factors can be calculated using $A_o\sqrt{H_o} / A_i$, where A_o and H_o are the area and height of the opening and A_i is the total area of the boundary surfaces.

^{vi} The main structural members were either made of cross laminated timber (CLT), nailed laminated timber (NLT) light timber frame assemblies (LTF) or light steel frame assemblies (LSF).

B.2 Maximum heat release rate and external flaming

Numerous correlations exist in the literature describing the maximum heat release rate that can be attained within a small enclosure in ventilation-controlled conditions. Herein, the common correlation noted in textbooks (Wickström, 2016) is adopted, i.e.:

$$\dot{Q}_{C,max,int} = \alpha_1 * \alpha_4 * A_o\sqrt{H_o} \quad \text{eq. B1}$$

Where α_4 is the energy released per unit mass of inflowing air ($3.01 * 10^6$ W s/kg, if supply air has an oxygen content of 23% - volume basis).

During the post-flashover fire, combustion can take place outside the ventilation opening, where outflowing combustibles will enter an oxygen-rich environment. The extent of external flaming is commonly expressed using an excess fuel fraction, α_4 . The excess fuel fraction can be defined as the ratio between the exterior heat release rate and the interior heat release rate.

$$\dot{Q}_{C,max,total} = \dot{Q}_{C,max,int} * (1 + \alpha_4) \quad \text{eq. B2}$$

Where $\dot{Q}_{C,max,total}$ is the maximum heat release rate of internal and external combustion combined.

B.3 Fire growth rate

The model presented in this paper aims to give a practical solution for the structural assessment of compartments exposed to fires. Brandon and Anderson (2018) showed, that the predicted damage after the full duration of an uncontrolled flashover fire is practically independent of the fire growth rate. As the pre-flashover fire is not the focus of the model, a fast fire growth rate of 0.047 kW/s², which corresponds well with the experimental results of flashover compartment fire tests of Table B.1, is assumed.

B.4 Combustion efficiency

In most fires, not all of the combustibles completely burn out. The combustion efficiency is the ratio between the variable fire load and the total heat released during a fire and can be determined as follows:

$$\alpha_5 = \frac{\int_0^{t_\infty} Q_C(t)dt}{F} \quad \text{eq. B3}$$

Where $Q_C(t)$ is the heat release rate as a function of time, t;

F is the total variable fire load.

All tests included in Table B.1 were stopped after a significant period of fire decay. However, none of the tests was performed until the heat release rate completely diminished. Therefore, it is not possible to determine the exact combustion efficiency from these results. However, it is determined that the combustion efficiency is commonly around 0.8. Therefore, a combustion efficiency of 0.8 is chosen for this study.

B.5 The decay phase and the start of decay

The start of a decay phase is often assumed to occur after a fraction of the fuel load, α_6 , is consumed by the fire. The reduction of the heat release rate is commonly assumed to follow a parabolic or linear function. However, assuming these types of functions generally leads to sudden a stop of the fire, which is too abrupt in comparison with compartment fires. Therefore, this study implements a hyperbolic function for the decay phase, which has the following form:

$$Q_{C;dec}(t) = \frac{1}{x(t-y)} \quad \text{eq. B4}$$

Where $Q_{C;dec}(t)$ is the heat release rate of the variable fire load during the decay phase as a function of time

t is the time

x and y are determined using the following boundary conditions:

- $\int_0^{t_{dec}} Q_C(t) dt = \alpha_5 \alpha_6 F$, as the total area under the heat release rate curve should correspond to the fuel load and the combustion efficiency.
- $Q_C(t_{dec}) = \dot{Q}_{C;max;total}$, as the heat release declines during the decay phase, from the heat release rate corresponding to the fully developed phase to zero.
- $\int_{t_{dec}}^{\infty} Q_{C;dec}(t) dt = \alpha_5(1 - \alpha_6)F$, as the area under the heat release rate curve of the decay phase should correspond to fuel left at the start of the decay and the combustion efficiency.

In the method discussed in Annex A.5, the energy of the char oxidation is added after flame extinction occurs. For that method the hyperbolic function of eq. B4 is interrupted at the temperature at which extinction of flaming combustion occurs. From that time onwards a new hyperbolic curve is used for which the area under the curve is increased with the energy of char oxidation.

B.6 Empirical constants

Values of α_1 and α_4 to α_6 and the maximum heat release rate per floor area of movable fuel (furnishings etc.) are needed to use the equations of this Annex. Some, but not all of these can be found in design standards. The values used in the main text of the report are determined empirically from compartment tests as discussed here. Only tests that

involved a full or nearly full duration of a flashover fire in compartments with typical apartment furniture were considered.

The experimental heat release rate curves for the purpose of benchmarking herein are those indicated in Table B.1, which were reported by McGregor (2014) and Li *et al.* (2014), Su and Loughheed (2014), Janssens (2016) and Chen (2008). Whilst some charring of the CLT was noted in some of these experiments, the contribution of the CLT to the fire loading was nominal in contrast to that of the variable fire loading. Therefore, the heat release rate measured can be considered representative of the heat release rate of the furniture within the fire enclosure. The design fire input parameters are chosen empirically, so that the predicted heat release rate curves correspond to those of the tests in Table B.1- The resulting parameters are summarised in Table B.2. Figure 19, Figure 20, Figure 21 and Figure 22 contrast the experimental data and the model input time-HRR relationship.

Table B.2: Empirically determined design fire curve parameters for compartments with typical apartment furniture and non-combustible linings

Fire growth rate (kW/s ²)	0.047
Flow rate coefficient, α_1 (kg/(s m ^{5/2}))	0.40
Excess fuel fraction, α_4 (-)	0.1
Combustion efficiency, α_5 (-)	0.8
Fraction of fuel load at start of decay, α_6 (-)	0.5
Maximum heat release rate density of movable fuel (kW/m ²)	320
<i>Note: Only tests F1 and F2 were fuel controlled according to the equations given in this Annex. The maximum heat release rate density was, therefore, only correlated to 2 tests. The maximum heat release rate density in accordance with Eurocode is 250 kW/m²</i>	

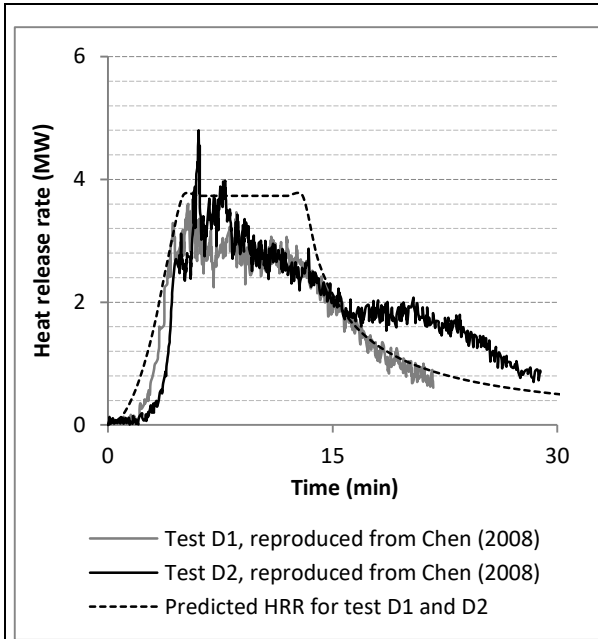


Figure 19: Experimental and model input heat release rates of test D1 and D2. Experimental results are reproduced from Chen (2018).

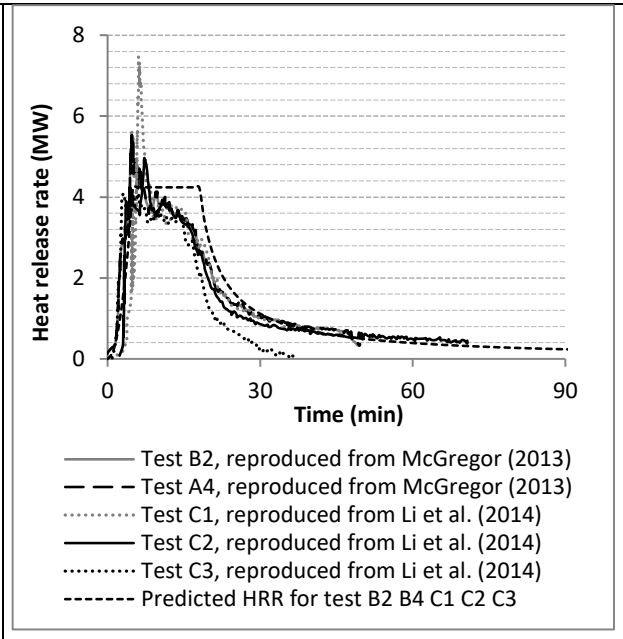


Figure 20: Experimental and model input heat release rates of Test B2, B4, C1, C2, C3. Experimental results are reproduced from McGregor (2014) and Li et al. (2014).

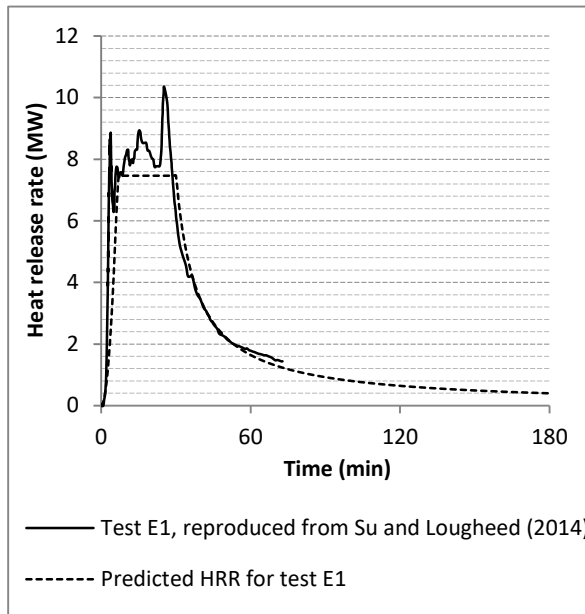


Figure 21: Experimental and model input heat release rates of test E1. Experimental results are reproduced from Su and Lougheed (2014).

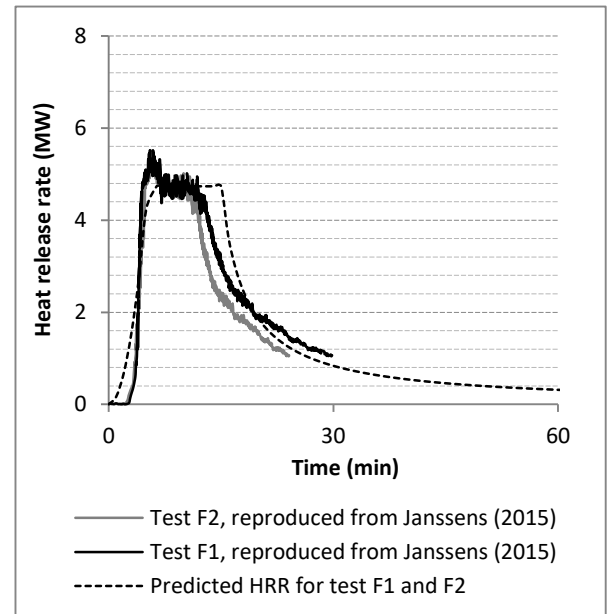


Figure 22: Experimental and model input heat release rate of test F1 and F2. Experimental results are reproduced from Janssens (2015).

Annex C: *a priori* modeling prediction results

In this Annex the modeling predictions that were sent to the project reference group before the test are set against the experimental results. No modeling predictions were made for Test 4 as the fire was not expected to have a well-mixed state of the fire, which is the primary assumption of a single zone model. For Test 1, 2, 3 and 5 the following was predicted:

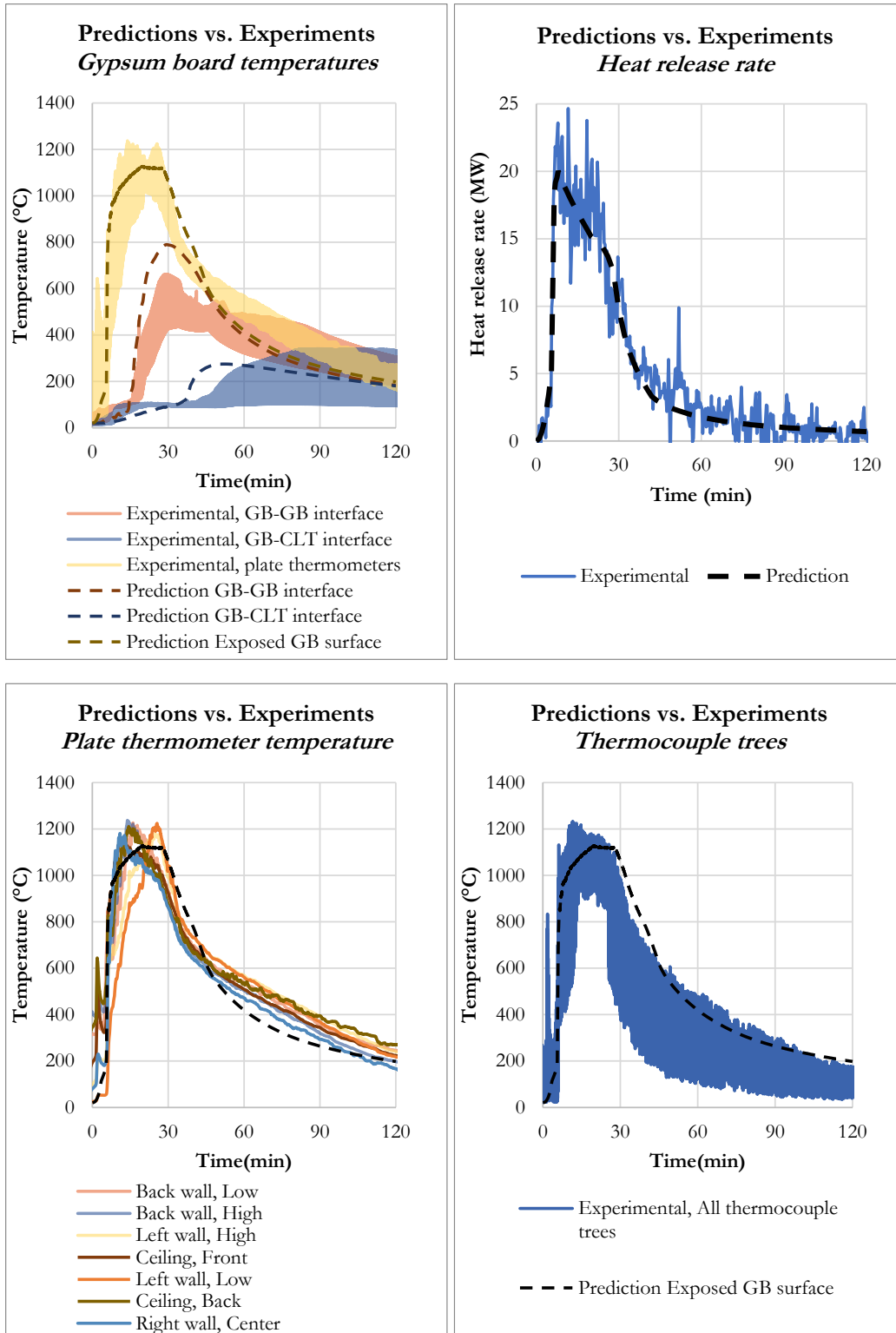
- The heat release rate for the fire duration
- Gas temperatures for the fire duration
- The temperatures behind each gypsum layer and potential prediction of fall-off of layers
- Whether charring would occur behind protected surfaces by assessing a temperature criterion of 300°C at the protected mass timber surface

The following sections give these predictions per test. The parameters used for these predictions were:

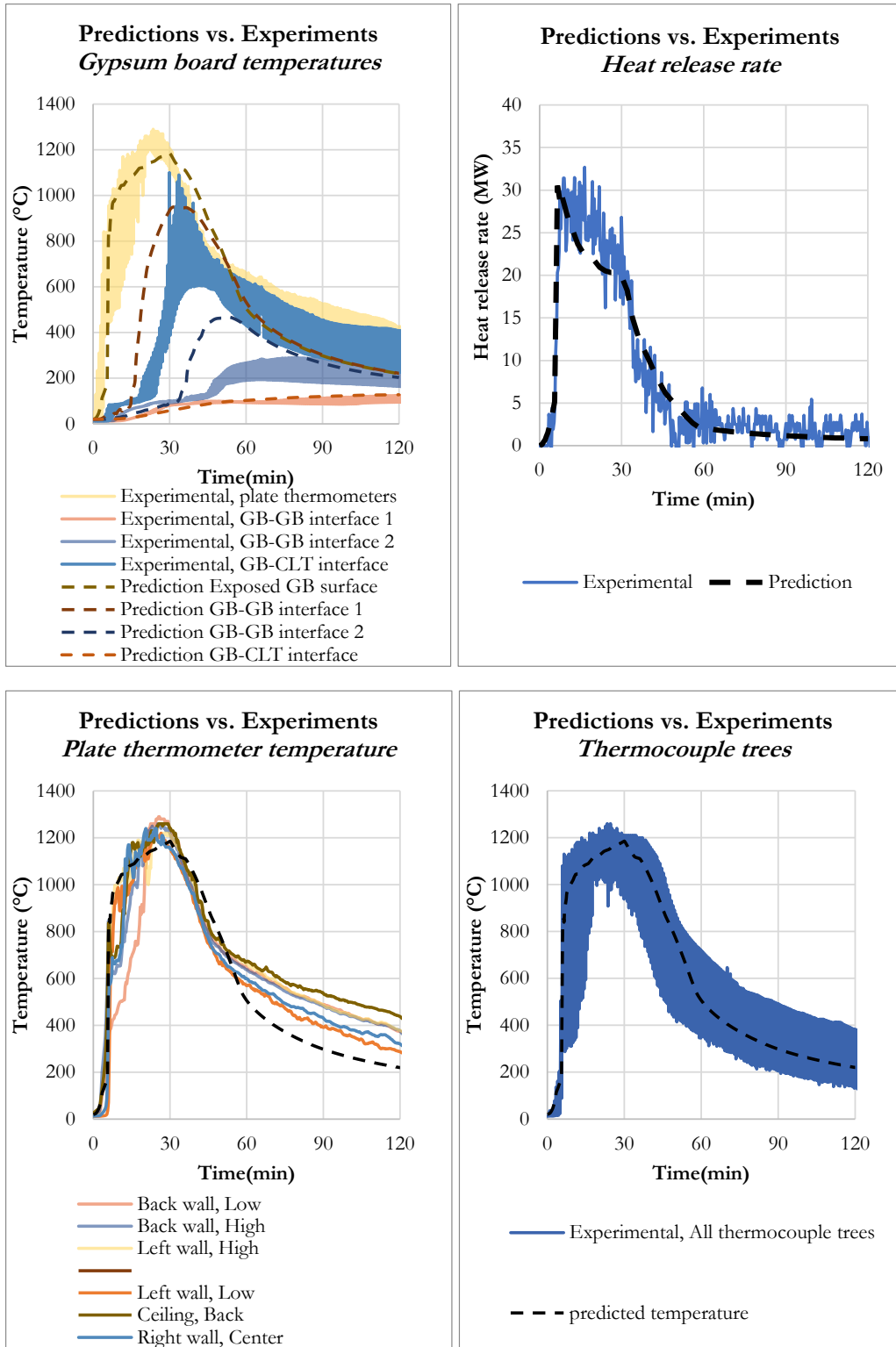
- Fuel load density: 560 MJ/m² (target of experiments)
- Heat release rate density: 190 kW/m² (note: this is lower than the updated predictions, which used 220 kW/m²)
- Portion of fuel used at start of decay: 60%

Char oxidation energy was added to the moveable fuel energy, which extended the fully developed phase but did not change the decay phase. The energy for char oxidation was determined from the quantity of timber combustion that could not take place within the stoichiometric limit. It was assumed that 30% of this energy was stored in the form of char, to be released when char oxidation was assumed to take place. This alteration was not implemented in the original report by Brandon and Andersson.

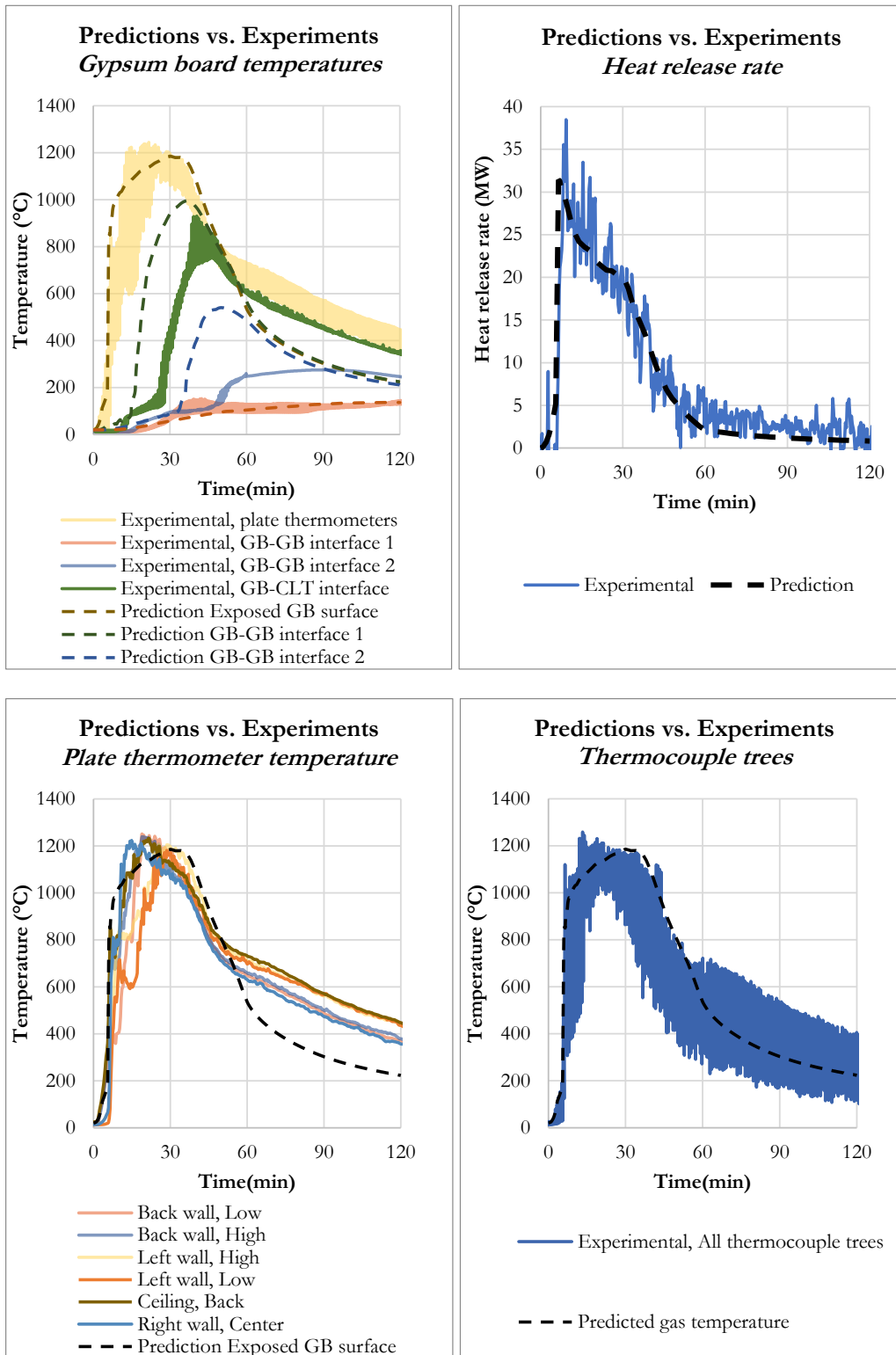
C.1 Test 1 *a priori* model predictions



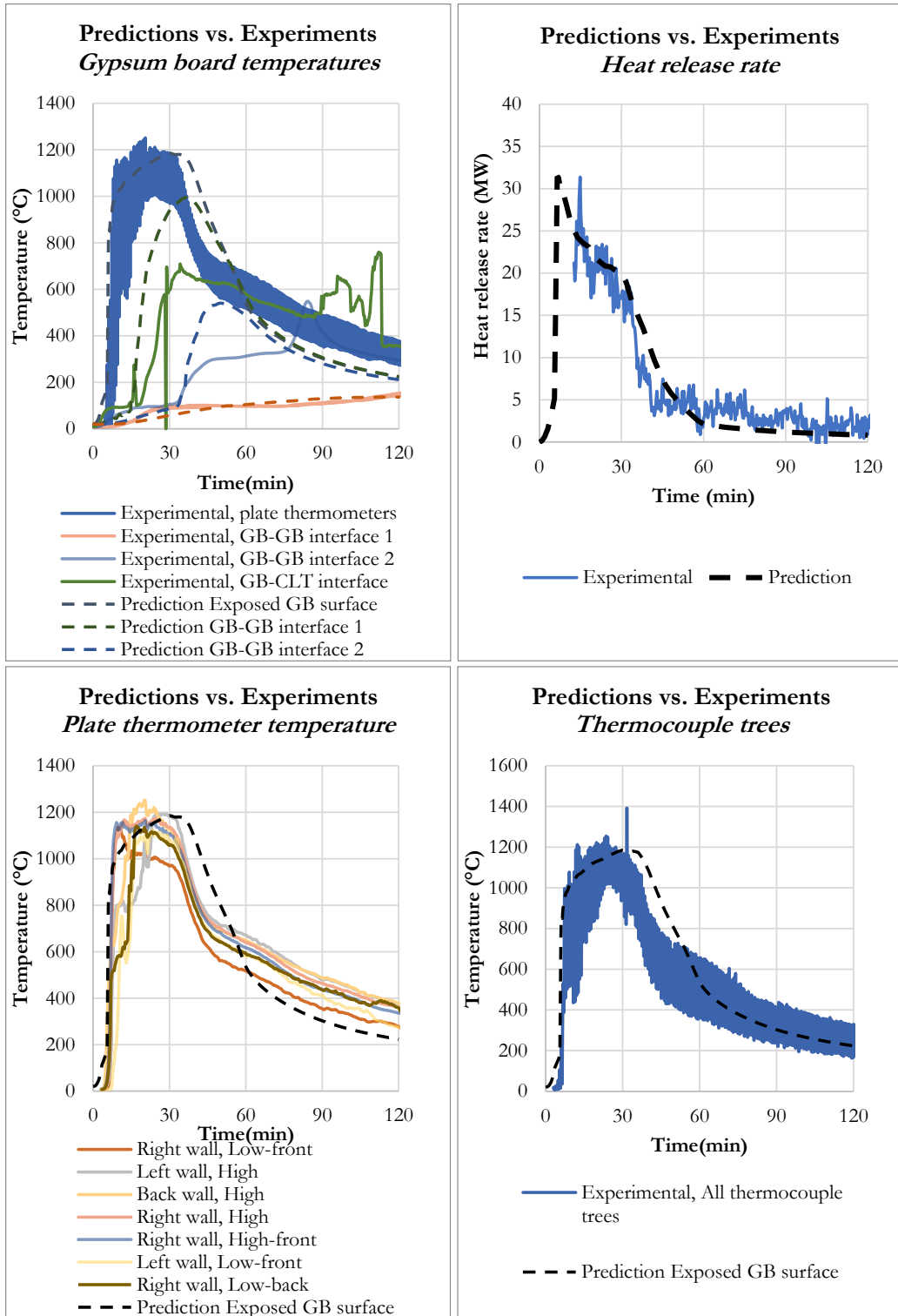
C.2 Test 2 *a priori* model predictions



C.3 Test 3 *a priori* model predictions



C.4 Test 5 *a priori* model predictions



Through our international collaboration programmes with academia, industry, and the public sector, we ensure the competitiveness of the Swedish business community on an international level and contribute to a sustainable society. Our 2,800 employees support and promote all manner of innovative processes, and our roughly 100 testbeds and demonstration facilities are instrumental in developing the future-proofing of products, technologies, and services. RISE Research Institutes of Sweden is fully owned by the Swedish state.

I internationell samverkan med akademi, näringsliv och offentlig sektor bidrar vi till ett konkurrenskraftigt näringsliv och ett hållbart samhälle. RISE 2 800 medarbetare driver och stöder alla typer av innovationsprocesser. Vi erbjuder ett 100-tal test- och demonstrationsmiljöer för framtidssäkra produkter, tekniker och tjänster. RISE Research Institutes of Sweden ägs av svenska staten.



RISE Research Institutes of Sweden AB
Box 857, 501 15 BORÅS, SWEDEN
Telephone: +46 10-516 50 00
E-mail: info@ri.se, Internet: www.ri.se

Fire Research
RISE Report 2021:63
ISBN: